nature neuroscience

PD-L1 inhibits acute and chronic pain by suppressing nociceptive neuron activity via PD-1

Gang Chen[1,2,6], Yong Ho Kim[1,3,6], Hui Li[4], Hao Luo[1,4], Da-Lu Liu[1], Zhi-Jun Zhang[1], Mark Lay[1], Wonseok Chang[1], Yu-Qiu Zhang[4] & Ru-Rong Ji[1,4,5]

Programmed cell death ligand-1 (PD-L1) is typically produced by cancer cells and suppresses immunity through the receptor PD-1 expressed on T cells. However, the role of PD-L1 and PD-1 in regulating pain and neuronal function is unclear. Here we report that both melanoma and normal neural tissues including dorsal root ganglion (DRG) produce PD-L1 that can potently inhibit acute and chronic pain. Intraplantar injection of PD-L1 evoked analgesia in naive mice via PD-1, whereas PD-L1 neutralization or PD-1 blockade induced mechanical allodynia. Mice lacking *Pd1* (*Pdcd1*) exhibited thermal and mechanical hypersensitivity. PD-1 activation in DRG nociceptive neurons by PD-L1 induced phosphorylation of the tyrosine phosphatase SHP-1, inhibited sodium channels and caused hyperpolarization through activation of TREK2 K^+ channels. PD-L1 also potently suppressed nociceptive neuron excitability in human DRGs. Notably, blocking PD-L1 or PD-1 elicited spontaneous pain and allodynia in melanoma-bearing mice. Our findings identify a previously unrecognized role of PD-L1 as an endogenous pain inhibitor and a neuromodulator.

Cancer pain markedly impairs the quality of life in patients. Breast, lung and prostate cancers frequently metastasize to bones and cause bone cancer pain by releasing algogenic substances. These substances include protons, bradykinin, endothelins, prostaglandins, proteases and growth factors such as nerve growth factor (NGF) and vascular endothelial growth factor (VEGF)[1–4] that can interact with peripheral nerves and cause increased hypersensitivity and excitability of nociceptive neurons (nociceptors)[3,5,6]. NGF and VEGF also induce outgrowth of pain-conducting nerve fibers in cancer affected areas[3,4]. Despite the focus on cancer-produced pronociceptive mediators[7], early-stage cancers before metastasis to bone are often not painful[2,8] and pain in melanoma is not common before metastasis[9]. It is conceivable that different cancers and even the same cancers at different growth stages may produce different pain mediators that can differentially regulate pain sensitivity via positive or negative modulation[10].

Mounting evidences suggests that cancers such as melanoma express the checkpoint inhibitory protein PD-L1 (CD274), which can suppress T cell function and induce immune tolerance via its receptor PD-1 (refs. 11–14). Emerging immune therapy such as anti-PD1 and anti-PD-L1 treatment has shown success in treating cancers such as melanoma[8,15,16], as well as lymphoma, lung cancer, ovarian cancer and head and neck cancers[17–19]. However, it is unclear whether and how the PD-L1–PD-1 pathway can regulate pain sensitivity via nonimmune means such as neuronal modulation. It is increasingly appreciated that primary nociceptors share similarities with immune cells and can both listen and talk to immune cells[10,20,21]. Nociceptors not only respond to immune mediators such as cytokines, chemokines and bacterial infection[22] but also produce cytokines and chemokines and express Toll-like receptors (TLRs), key regulators of immunity[20,23–25]. In primary sensory neurons, TLRs rapidly regulate pain sensitivity by interacting with ion channels[10,26]. It remains unclear whether nociceptive neurons express functional PD-1 receptor, an important immune regulator, in mouse and human DRG.

We assessed the expression and function of PD-1 in primary sensory neurons of mouse and human DRG. We found that activation of PD-1 by PD-L1 potently suppressed neuronal activities in mouse and human nociceptive neurons. Moreover, PD-L1 inhibited acute baseline pain and inflammatory pain and chronic neuropathic pain after nerve injury. In addition to malignant melanoma tissue, we detected endogenous PD-L1 in normal neural tissues, including spinal cord, DRG and nerve, as well as skin. We also discovered that PD-L1 potently suppressed spinal cord synaptic transmission in the pain circuit as a neuromodulator. Finally, PD-L1 masked pain in melanoma, and conversely, blocking PD-L1 or PD-1 elicited spontaneous pain and allodynia in melanoma-bearing mice.

RESULTS

PD-L1 inhibits acute inflammatory pain and increases pain threshold in naive animals

As a first step to address the function of PD-L1 in acute pain modulation, we examined the effects of PD-L1 in an acute inflammatory pain model. Intraplantar (i.pl.) injection of formalin (5%) induced

[1]Department of Anesthesiology, Duke University Medical Center, Durham, North Carolina, USA. [2]Key Laboratory of Neuroregeneration of Jiangsu and Ministry of Education, Co-Innovation Center of Neuroregeneration, Nantong University, Nantong, Jiangsu, China. [3]Department of Physiology, College of Medicine, Gachon University, Incheon, Republic of Korea. [4]Institute of Neurobiology, Institutes of Brain Science and State Key Laboratory of Medical Neurobiology, Collaborative Innovation Center for Brain Science, Fudan University, Shanghai, China. [5]Department of Neurobiology, Duke University Medical Center, Durham, North Carolina, USA. [6]These authors contributed equally to this work. Correspondence should be addressed to R.-R.J. (ru-rong.ji@duke.edu) or Y.-Q.Z. (yuqiuzhang@fudan.edu.cn).

Received 7 February; accepted 27 April; published online 22 May 2017; doi:10.1038/nn.4571

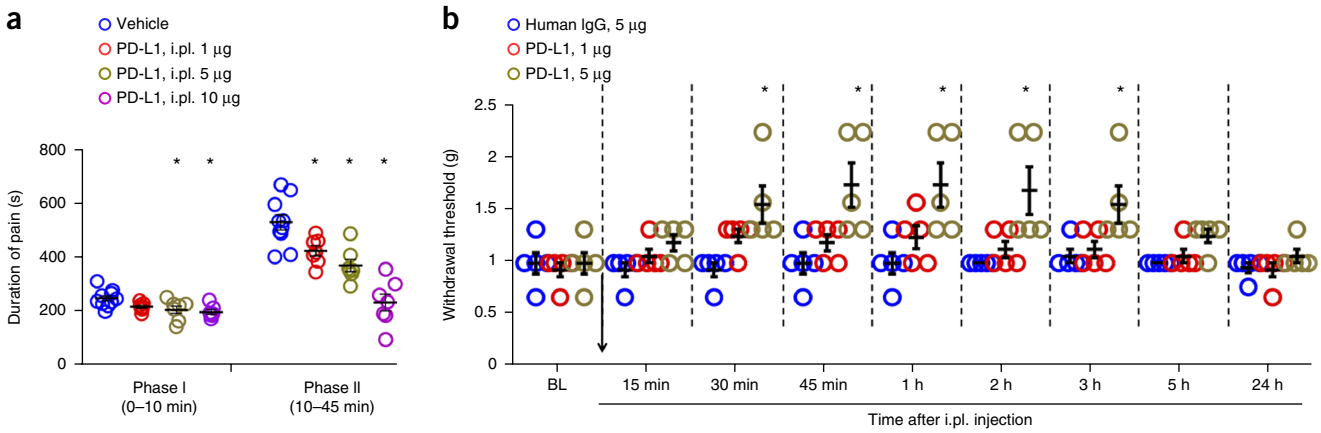

Figure 1 Exogenous PD-L1 inhibits formalin-induced inflammatory pain and increases pain threshold in naive mice. (**a**) Formalin-induced first-phase and second-phase inflammatory pain, as measured by duration of spontaneous pain behavior (flinching or licking) in each interval of 5 min, is reduced by i.pl. pretreatment with PD-L1 (1–10 μg). *$P < 0.05$ versus vehicle (PBS), one-way ANOVA (phase 1: $P = 0.0065$; phase 2: $P = 0.0001$), $n = 7$–10 mice per group. PD-L1 was administered 30 min before the formalin injection. (**b**) Basal mechanical pain assessed by von Frey test in naive mice. There is an increase in paw withdrawal threshold after PD-L1 injection (1 and 5 μg, i.pl.). $P = 0.0319$, repeated-measures two-way ANOVA, followed by Bonferroni's *post hoc* test, *$P < 0.05$ versus human IgG, $n = 5$ mice per group. Arrow indicates drug injection. Data are mean ± s.e.m.

typical biphasic inflammatory pain, as previously reported[27], but the second-phase pain (10–45 min) was substantially inhibited by PD-L1 pretreatment (i.pl., 1–10 μg, $P < 0.05$, one-way ANOVA), in a dose-dependent manner (**Fig. 1a**). At high doses (5 and 10 μg), PD-L1 also caused a mild inhibition of the first-phase pain (**Fig. 1a**).

Next we tested whether PD-L1 would also alter pain threshold in naive mice. The von Frey test revealed a significant increase in paw withdrawal threshold after i.pl. injection of PD-L1 (5 μg, ~0.1 nmol, $P < 0.05$, two-way ANOVA). The threshold increase was rapid and evident at 30 min and was maintained for 3 h after the injection (**Fig. 1b**). Since we injected a chimeric PD-L1 fusion protein with human immunoglobulin G (IgG) at the C terminus, we used human IgG as an inactive control. This human IgG had no effect on the pain threshold (**Fig. 1b**).

PD-L1 is an endogenous pain inhibitor and alters basal pain thresholds via PD-1

PD-L1 is produced by malignant tissues and serves as a predictive biomarker in cancer immunotherapy[28]. As expected, mouse B16 melanoma tissue has high expression of PD-L1 (~450 ng/mg tissue, **Fig. 2a**), as evaluated by ELISA. PD-L1 was also secreted in culture medium of melanoma cells (**Supplementary Fig. 1a**). To determine whether normal tissues also produce PD-L1, we compared PD-L1 contents in non-neural and neural tissues. Non-neural tissues, such as liver, spleen and kidney, had high levels of PD-L1 (~70–90 ng/mg tissue; **Fig. 2a**). Neural tissues, including brain, spinal cord and DRG had PD-L1 levels around 50 ng/mg tissue (**Fig. 2a**). Furthermore, we detected PD-L1 in the sciatic nerve and hindpaw skin tissues (**Fig. 2a**), which contain pain-sensing nerve fibers. These results suggest that PD-L1 is broadly synthesized by neural and skin tissue. In agreement, *in situ* hybridization revealed *Pdl1* mRNA expression in mouse DRG neurons (**Supplementary Fig. 1b**,**c**).

To determine whether endogenous PD-L1, produced by nonmalignant tissues, regulates pain, we tested mechanical pain after pharmacological blockade of either PD-L1 or PD-1 in naive mice. Neutralization of hindpaw PD-L1 by i.pl. injection of soluble PD-1 (sPD-1, 5 μg, ~0.1 nmol) induced a transient mechanical allodynia for 3 h (**Fig. 2b**), without causing spontaneous pain

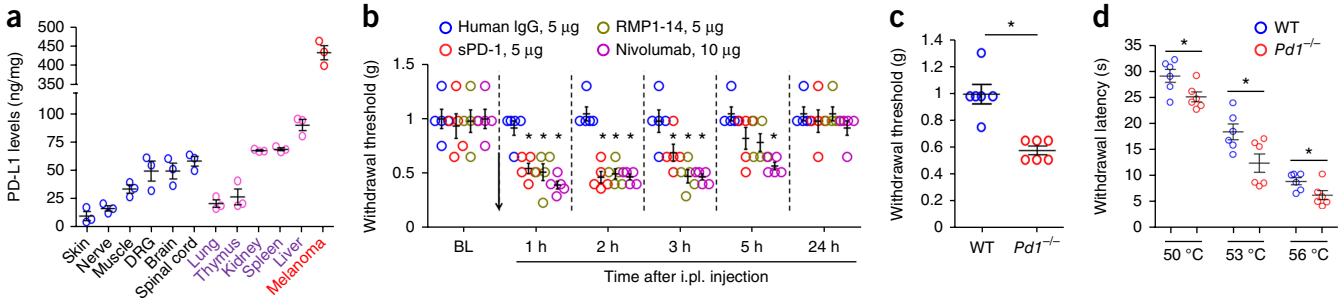

Figure 2 Endogenous PD-L1 regulates pain sensitivity in naive mice via PD-1. (**a**) ELISA analysis showing endogenous expression of PD-L1 in nonmalignant tissues of naive mice and melanoma tissue removed from a mouse hindpaw 4 weeks after melanoma cell inoculation. PD-L1 is widely expressed in various nonmalignant tissues. $n = 3$ mice per group. (**b**) Inhibition of endogenous PD-L1 and PD-1 induces mechanical allodynia in naive mice. PD-L1 was neutralized with sPD-1 (5 μg, i.pl.), and PD-1 was blocked by monoclonal antibodies RMP1-14 (mouse anti-PD-1 antibody, 5 μg, i.pl.) and nivolumab (human anti-PD-1 antibody, 10 μg, i.pl.). $P = 0.0007$, repeated-measures two-way ANOVA, followed by Bonferroni's *post hoc* test, *$P < 0.05$, versus human IgG, , $n = 5$ mice per group. Arrow indicates drug injection. (**c**,**d**) Reduced mechanical and thermal pain threshold in $Pd1^{-/-}$ mice, as shown in von Frey test (**c**) and hot plate test (**d**). *$P = 0.0003$ (**c**); $P = 0.0288$, 0.0268 and 0.0397 for 50, 53, and 56 °C, respectively (**d**); two-tailed Student's *t*-test, $n = 6$ mice per group. Data are mean ± s.e.m.

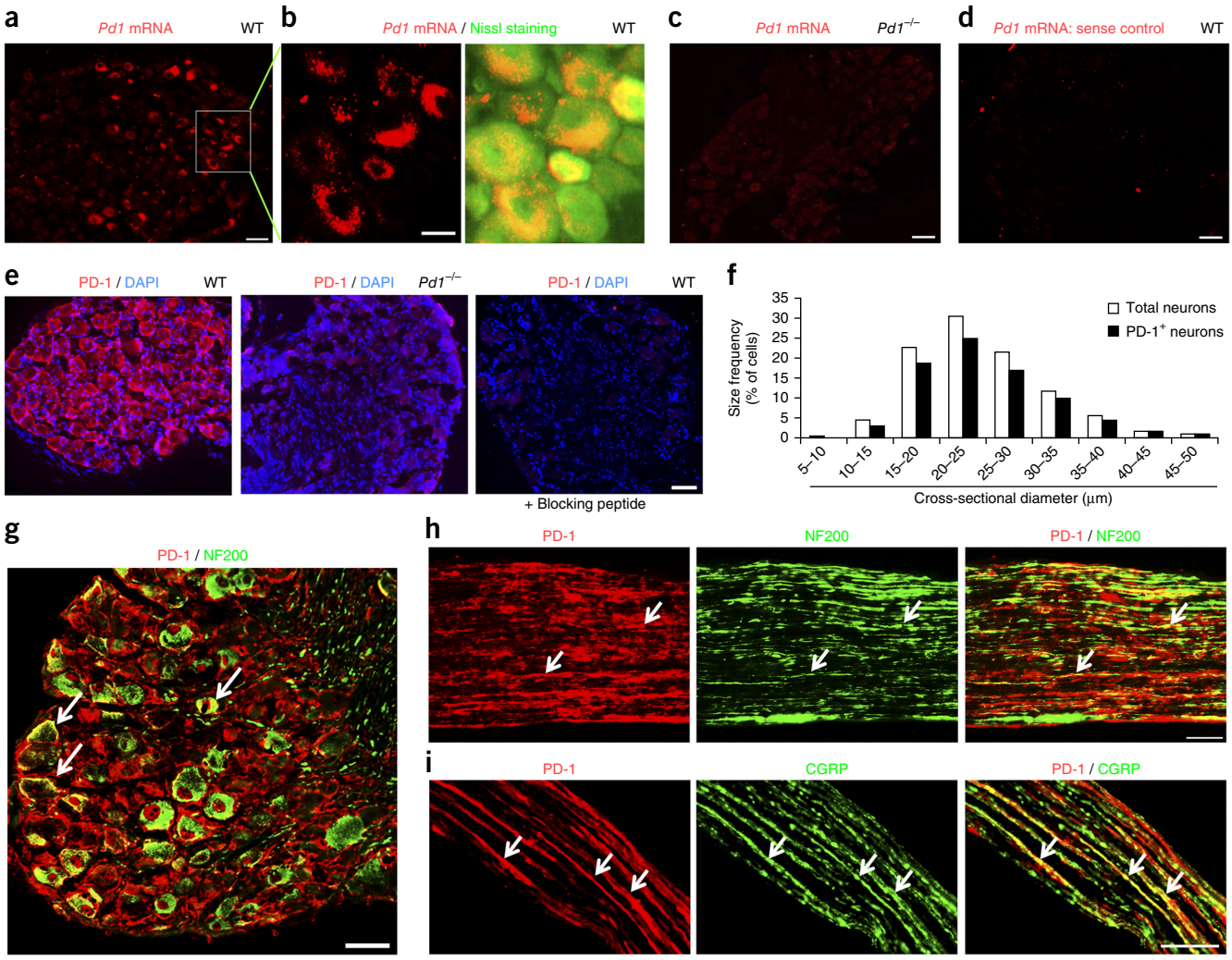

Figure 3 PD-1 is expressed by mouse DRG neurons and nerve axons. (**a**–**d**) *In situ* hybridization (ISH) images showing *Pd1* mRNA expression in DRG of WT but not *Pd1*$^{-/-}$ mice. (**a**) Low-magnification image of ISH with antisense probe showing *Pd1* mRNA in DRG neurons of WT mice. Scale bar, 50 μm. (**b**) High-magnification image of ISH (red) and Nissl staining (green) in DRG sections. Scale bar, 20 μm. (**c**) ISH image showing loss of *Pd1* mRNA expression in DRG neurons in *Pd1*$^{-/-}$ mice. Scale bar, 50 μm. (**d**) ISH image of sense control probe. Scale bar, 50 μm. (**e**) Left, image of immunostaining showing broad PD-1 expression in mouse DRG neurons. Middle, PD-1 expression is lost in *Pd1*$^{-/-}$ mice. Right, absence of PD-1 immunostaining upon treatment with a blocking peptide. Blue DAPI staining shows all cell nuclei in DRG sections. Scale bar, 50 μm. (**f**) Size frequency distribution of PD-1-positive and total neurons in mouse DRGs. A total of 1,555 neurons from 4 WT mice were analyzed. (**g**,**h**) Double staining for PD-1 and NF200 in DRG (**g**) and sciatic nerve (**h**) sections of mice. PD-1 is expressed in both NF200-positive and NF200-negative DRG neurons and sciatic nerve axons. Scale bars, 50 μm. (**i**) Double immunostaining for PD-1 and CGRP in mouse sciatic nerve. PD-1 is present in axons coexpressing CGRP. Scale bar, 50 μm. Arrows in **g**–**i** indicate the double-labeled neurons and axons.

(**Supplementary Fig. 2a**). Blockade of PD-1 with a mouse anti-PD-1 antibody, RMP1-14 (5 μg, ~0.1 nmol, i.pl.), also induced mechanical allodynia for 3 h (**Fig. 2b**).

Nivolumab (Opdivo) is a US Food and Drug Administration–approved fully humanized IgG4 monoclonal antibody that selectively targets PD-1 (ref. 29) and has shown success in treating melanoma, lymphoma and lung cancer[17,29,30]. Of note, nivolumab (10 μg, ~0.07 nmol, i.pl.), but not control human IgG, induced marked mechanical allodynia for 5 h (**Fig. 2b**). PD-L1's analgesic effects were blocked by both RMP-14 and nivolumab (**Supplementary Fig. 2b**), suggesting that PD-L1 inhibits pain via PD-1. As a human antibody, nivolumab showed cross-reactivity in mouse tissue and binding to DRG neurons and sciatic nerve fibers in wild-type (WT) mice. This binding was absent in *Pd1* knockout mice (*Pd1*$^{-/-}$; **Supplementary Fig. 2c**).

Next we tested baseline pain and PD-L1-induced analgesia in *Pd1*$^{-/-}$ mice with and without PD-L1 treatment. Notably, baseline pain sensitivity was elevated in naive *Pd1*$^{-/-}$ mice. Compared with WT mice, *Pd1*$^{-/-}$ mice displayed mechanical and thermal hypersensitivity, showing decreased mechanical and thermal pain thresholds in the von Frey test and hot plate test (**Fig. 2c**,**d**). This result indicates that PD-1 regulates basal pain sensitivity. As expected, both the PD-L1-induced analgesic effect and RMP1-14-induced hyperalgesic effect were abolished in *Pd1*$^{-/-}$ mice (**Supplementary Fig. 3a**,**b**). Notably, *Pd1*$^{-/-}$ mice showed no developmental defects in sensory neurons and their innervations. The central innervations of primary afferents in the spinal cord dorsal horn were comparable in WT and knockout mice (**Supplementary Fig. 4**). The distribution patterns of primary sensory neurons, including small-sized nociceptive neurons (CGRP^{+} peptidergic neurons and IB4^{+} nonpeptidergic neurons)

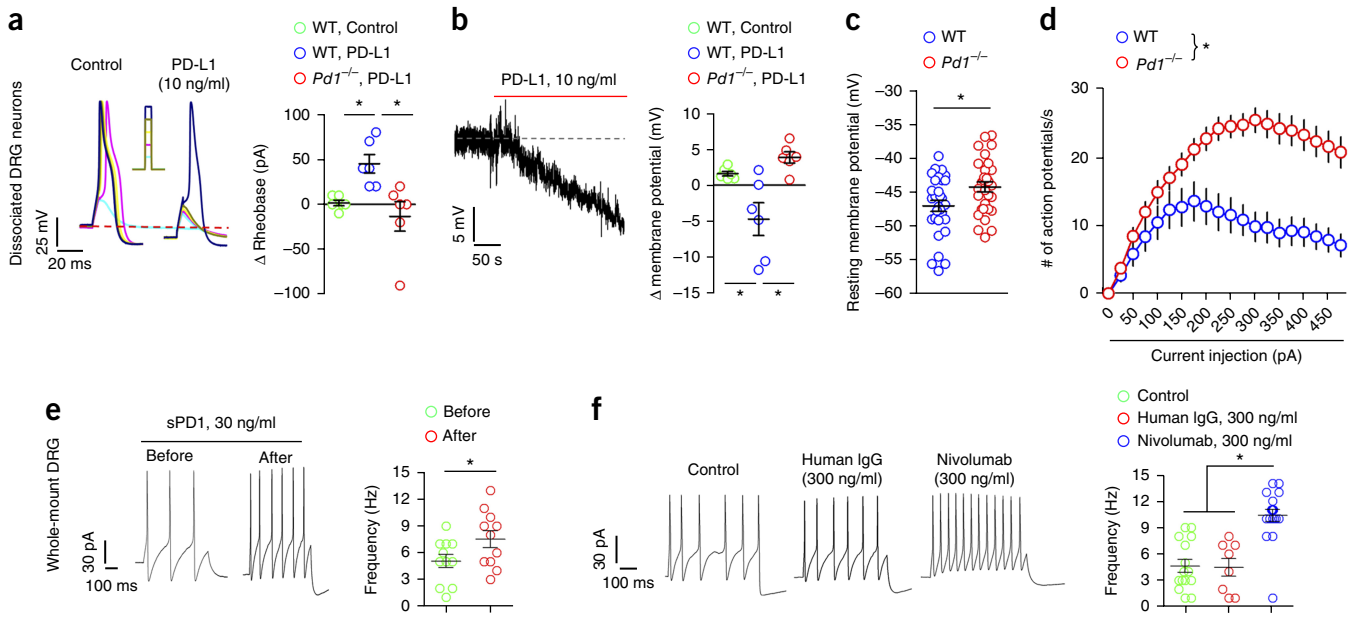

Figure 4 PD-L1 suppresses neuronal excitability in mouse DRG neurons via PD-1. (**a**–**f**) Patch clamp recordings in dissociated (**a**–**d**) and whole-mount (**e**,**f**) mouse DRG neurons with small diameters (<25 µm). (**a**) Left, action potential traces showing an inhibitory effect of PD-L1 (10 ng/ml) in WT neurons. Current injection for action potential induction starts from +10 pA and increases 10 pA per step. Right, rheobase change in WT and *Pd1*$^{-/-}$ mice. $P = 0.0062$, one-way ANOVA, followed by Bonferroni's *post hoc* test, $^{*}P < 0.05$, $n = 6$ neurons from 2 mice. (**b**) PD-L1 induces RMP hyperpolarization. Right, change of RMP in WT and *Pd1*$^{-/-}$ mice. $P = 0.0017$, one-way ANOVA, followed by Bonferroni's *post hoc* test, $^{*}P < 0.05$, $n = 6$ neurons from 2 mice. PD-L1 fails to suppress action potentials (**a**) and alter RMP (**b**) in *Pd1*$^{-/-}$ mice. (**c**,**d**) Altered RMP and increased excitability in DRG neurons of *Pd1*$^{-/-}$ mice. (**c**) RMP in WT and *Pd1*$^{-/-}$ mice. $^{*}P = 0.0149$, unpaired two-tailed *t*-test, $n = 30$ neurons from 2 mice. (**d**) Number of action potentials evoked by current injection in WT and *Pd1*$^{-/-}$ mice. $^{*}P = 0.0001$, two-way ANOVA, $n = 30$ neurons from 2 mice. (**e**) Whole-mount DRG recording showing increased action potential firing in small-sized DRG neurons after perfusion of sPD-1 (30 ng/ml). Left, traces of evoked action potentials before and after sPD-1 perfusion. Right, action potential frequency following sPD-1 perfusion. $^{*}P = 0.0143$, paired two-tailed Student's *t*-test, $n = 11$ neurons from 3 mice. (**f**) Whole-mount DRG recording showing increased action potential firing in small-sized neurons following nivolumab incubation (2 h, 300 ng/ml). Left, traces of evoked action potential in neurons incubated with control (artificial cerebrospinal fluid), human IgG and nivolumab. Right, frequency of action potentials showing the effects of human IgG and nivolumab. $P = 0.0001$, one-way ANOVA, followed by Bonferroni's *post hoc* test, $^{*}P < 0.05$ versus control and human IgG, $n = 8$–18 neurons from 3 mice. Data are mean ± s.e.m.

and large-sized A-fiber DRG neurons (NF200^{+}), as well as the total population of sensory neurons, were also unaltered in DRG tissues of knockout mice (**Supplementary Fig. 5**). Taken together, these findings in WT and *Pd1*$^{-/-}$ mice strongly suggest that (i) PD-L1 is an endogenous inhibitor of pain, (ii) PD-L1 produces analgesia via PD-1, and (iii) altered pain sensitivity in *Pd1*$^{-/-}$ mice is not a result of developmental defects in sensory neurons.

PD-1 receptor is expressed by primary sensory neurons in mouse DRGs

To determine peripheral mechanisms by which PD-L1 modulates pain, we examined *Pd1* mRNA and PD-1 protein expression in mouse DRG neurons. *In situ* hybridization showed *Pd1* mRNA expression in most DRG neurons, regardless of size (**Fig. 3a**,**b**). This signal was absent in *Pd1*$^{-/-}$ mice (**Fig. 3c**) and in DRG sections treated with sense control probe (**Fig. 3d**), confirming the specificity of *Pd1* mRNA expression. Immunohistochemistry revealed PD-1 immunoreactivity in most DRG neurons (**Fig. 3e**). The specificity of the PD-1 antibody was validated by loss of PD-1 immunostaining in DRG neurons of *Pd1*$^{-/-}$ mice (**Fig. 3e**) and further confirmed by absence of staining in WT DRG after co-incubation of the antibody with a blocking peptide (**Fig. 3e**). Size frequency analysis showed a broad expression of PD-1 by DRG neurons with small, medium and large sizes (**Fig. 3f**). Double staining confirmed PD-1 expression in both large-diameter A-fiber neurons (NF200^{+}) and small-diameter C-fiber neurons (NF200^{-}, **Fig. 3g**). PD-1 immunoreactivity was present in NF200^{+} and NF200^{-} axons in the sciatic nerve, indicating axonal transport of PD-1 from DRG cell bodies to peripheral axons (**Fig. 3h**). PD-1-immunoreactive axons coexpressed CGRP, a marker for nociceptive peptidergic neurons (**Fig. 3i**). Together, these results demonstrate that primary sensory neurons, including nociceptors and their axons, express PD-1, providing a neuronal basis for PD-1 modulation of pain.

PD-L1 suppresses nociceptive neuron activity in mouse DRGs via PD-1

Activation and sensitization of nociceptive sensory neurons (nociceptors) often produces pain and pain hypersensitivity[31–33]. We postulated that PD-L1–PD-1signaling inhibits pain via direct modulation of nociceptor activity. We used patch clamp recordings to evaluate excitability in dissociated small-diameter neurons (<25 µm, presumably nociceptors) in mouse DRGs. Notably, PD-L1, at a very low concentration (10 ng/ml, ~0.2 nM), evoked a potent and immediate inhibition of action potentials, induced by current injection, and also increased the rheobase, a minimum current to induce action potential (**Fig. 4a**). PD-L1 also induced hyperpolarization of the resting membrane potential (RMP) in DRG neurons (**Fig. 4b**). These effects of PD-L1 on action potentials and RMPs were abrogated in *Pd1*$^{-/-}$ mice, indicating that PD-L1 modulates neuronal excitability through PD-l (**Fig. 4a**,**b**). Furthermore, *Pd1*-deficient nociceptive neurons displayed increased RMP and firing frequency of action potentials (**Fig. 4c**,**d**), suggesting that the intrinsic excitability of nociceptors is enhanced in *Pd1* mutant mice.

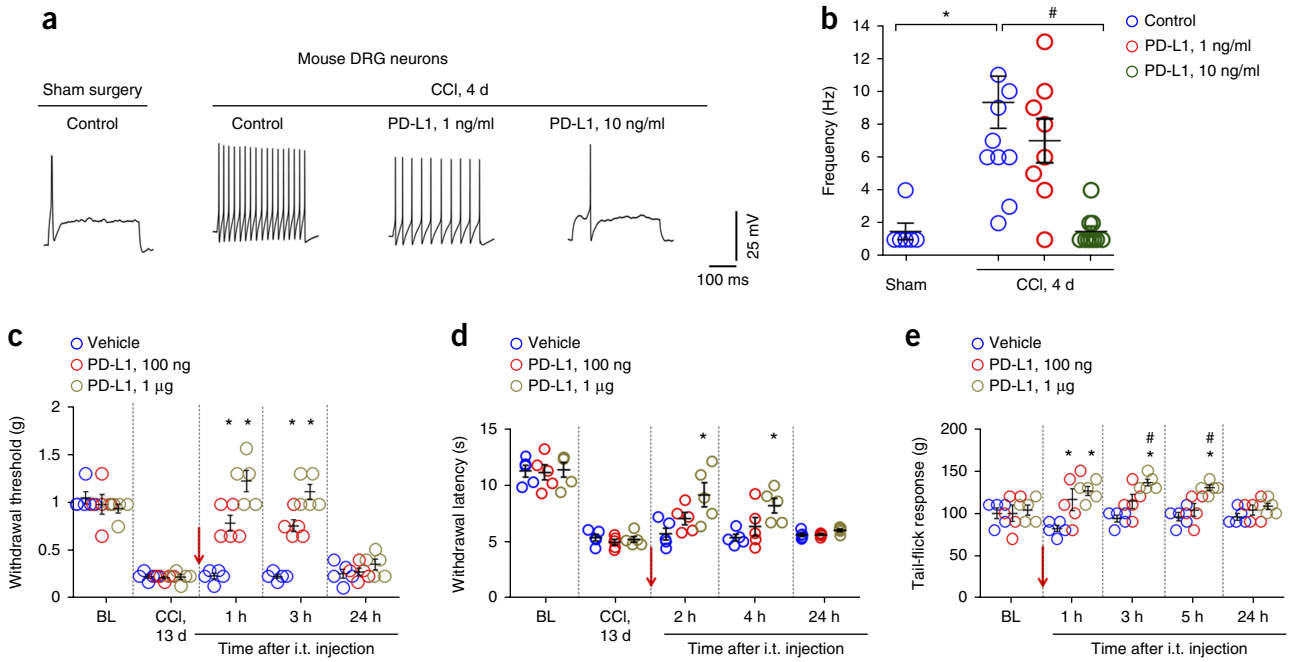

Figure 5 PD-L1 inhibits neuronal hyperexcitability and neuropathic pain after nerve injury. (**a**,**b**) PD-L1 blocks CCI-induced increases in action potential frequency in small-diameter neurons of whole-mount DRG. (**a**) Traces of action potentials 4 d after CCI and the effects of PD-L1 (1 and 10 ng/ml). (**b**) Frequency of action potentials. $P = 0.0023$, one-way ANOVA, followed by Bonferroni's *post hoc* test, $^{*}P = 0.0075$ versus sham control, $^{\#}P < 0.05$ versus control (no treatment), $n = 6$–9 neurons per group. (**c**,**d**) Intrathecal PD-L1 inhibits CCI-induced mechanical allodynia (**c**) and thermal hyperalgesia (**d**). $P = 0.0001$ (**c**), $P = 0.0199$ (**d**), repeated-measures two-way ANOVA, followed by Bonferroni's *post hoc* test, $^{*}P < 0.05$ versus vehicle, $n = 5$ mice per group. Arrow indicates drug injection. (**e**) Randall-Selitto test showing increased baseline mechanical pain threshold after intrathecal PD-L1 injection in naive mice. $P = 0.0240$, repeated-measures two-way ANOVA, followed by Bonferroni's *post hoc* test, $^{*}P < 0.05$ versus vehicle, $^{\#}P < 0.05$ versus baseline (BL), $n = 5$ mice per group. Arrow indicates drug injection. Data are mean ± s.e.m.

To further assess the contribution of endogenous PD-L1 and PD-1 to neuronal excitability in WT neurons, we used pharmacological approaches in a whole-mount DRG preparation. Compared to dissociated DRG neurons, the whole-mount DRG preparation has the advantage of retaining extracellular PD-L1. Neutralization of PD-L1 with sPD-1 (30 ng/ml, ~0.6 nM) increased the firing rate of action potentials in small-diameter DRG neurons (**Fig. 4e**). Blocking the function of PD-1 with nivolumab, but not the control IgG (300 ng/ml, ~2 nM), also increased the firing rate (**Fig. 4f**). Together, both gain-of-function and loss-of-function approaches demonstrate that PD-L1 and PD-1 are critical in regulating excitability of nociceptive neurons.

PD-L1 inhibits neuronal hyperexcitability and neuropathic pain after nerve injury

Hyperexcitability of primary sensory neurons after nerve injury has been strongly implicated in chronic pain[31,33–35]. We used the whole-mount mouse DRG preparation to examine hyperexcitability in small-sized nociceptive neurons after chronic nerve constriction injury (CCI). As expected, nociceptive neurons fired more action potentials after CCI (**Fig. 5a**). Notably, nerve injury-induced hyperexcitability (increased firing rate of action potentials) of DRG neurons was dose-dependently suppressed by PD-L1 (1–10 ng/ml, ~0.02–0.2 nM; **Fig. 5a**,**b**).

The central axons of nociceptive neurons terminate in the spinal cord dorsal horn to form first-order synapses in the pain pathway[33]. PD-L1 in DRG neurons could be transported to central axon terminals to modulate spinal cord synaptic transmission and nociception. To test this hypothesis, we examined the effects of intrathecal (i.t.) injection of PD-L1 on CCI-induced neuropathic pain in mice. PD-L1 reduced the CCI-induced mechanical allodynia at a low dose (100 ng; **Fig. 5c**). PD-L1 also significantly reduced CCI-induced heat hyperalgesia at a high dose (1 µg, $P < 0.05$, two-way ANOVA, **Fig. 5d**). The Randall-Selitto test further revealed that intrathecal PD-L1 increased paw withdrawal threshold in naive mice (**Fig. 5e**).

PD-L1 inhibits synaptic transmission and injury-induced neuronal hyperactivities in the spinal cord

Patch clamp recordings in spinal cord slices showed that superfusion of PD-L1 rapidly (within 1 min) reduced the frequency and amplitude of spontaneous EPSCs (sEPSCs) in lamina IIo neurons (**Supplementary Fig. 6a**). These interneurons form a nociceptive circuit with C-fiber afferents and projection neurons[36,37]. By sharp contrast, exposure of spinal cord slices to sPD-1 (PD-L1 neutralization) and nivolumab (PD-1 blockade) increased sEPSC frequency in lamina IIo neurons (**Supplementary Fig. 6b**,**c**). As expected, PD-L1's inhibition of sEPSC frequency was blocked by nivolumab (**Supplementary Fig. 6d**). Thus, PD-L1–PD-1 signaling also has an active role in modulating spinal nociceptive transmission.

Next we tested the central effects of PD-L1 in a bone cancer model in rats[38]. PD-L1, given two weeks after tumor cell inoculation via i.t. route, reduced bone cancer-induced mechanical allodynia ($P < 0.05$, two-way ANOVA, **Supplementary Fig. 7a**). Moreover, bone cancer-induced hyperexcitability of wide dynamic range (WDR) neurons in dorsal horn neurons was suppressed by PD-L1 (**Supplementary Fig. 7b**,**c**), whereas nivolumab enhanced activities of WDR neurons (**Supplementary Fig. 7d**,**e**). Taken together, our data suggest that PD-L1 is a neuromodulator in both the peripheral and central nervous system; and in the spinal cord PD-L1 regulates acute and chronic pain by suppressing nociceptive synaptic transmission and injury-induced neuronal plasticity in dorsal horn neurons via PD-1 receptor.

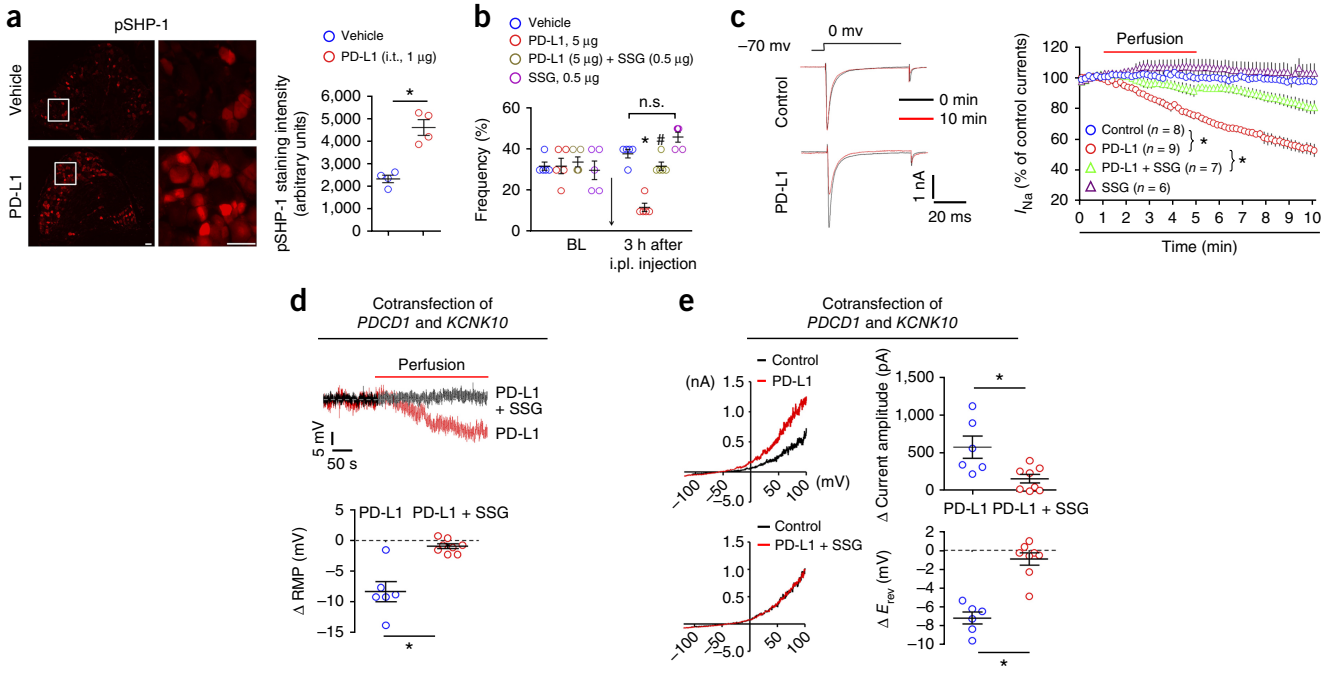

Figure 6 PD-L1 modulates neuronal excitability and pain via SHP-1. (**a**) Intrathecal PD-L1 (i.t. 1 μg, 30 min) increased phosphorylation of SHP-1 (pSHP-1) in mouse DRG neurons. Left, images of pSHP-1 immunostaining in vehicle- and PD-L1-treated groups. Scale bar, 50 μm. Middle, enlarged images from the boxes. Scale bar, 50 μm. Right, immunofluorescence intensity of pSHP-1 in neurons. $^{*}P = 0.001$, two-tailed *t*-test, $n = 4$ mice per group. (**b**) Paw withdrawal frequency to a 0.6 g filament in naive mice and the effects of i.pl. SSG (SHP-1 inhibitor), PD-L1, and PD-L1 plus SSG in naive mice. Note that PD-L1-induced analgesia is abolished by SSG. $P = 0.0001$, one-way ANOVA, followed by Bonferroni's *post hoc* test, $^{*}P < 0.05$ versus vehicle (PBS); $^{\#}P < 0.05$ versus PD-L1; n.s., no significance;, $n = 5$ mice per group. (**c**) Inhibition of transient sodium currents by PD-L1 (10 ng/ml) in dissociated DRG neurons and the effect of SSG (11 μM). Left, traces of sodium currents. Right, time course of relative sodium currents. $^{*}P = 0.0001$, two-way repeated-measures ANOVA(), $n = 6$–9 neurons from 2 mice. (**d**) Regulation of RMP by PD-L1 (10 ng/ml) and its blockade by SSG (11 μM) in CHO cells. $^{*}P = 0.0007$, two-tailed Student's *t*-test, $n = 6$–8 cells from 2 cultures. (**e**) PD-L1 increases TREK2 activity via SHP-1 in CHO cells. Left, traces of TREK2-induced outward currents and the effects of PD-L1 and SSG. Right, quantification of outward currents and RMP changes; E_{rev}, reversal potential. $^{*}P = 0.0128$ (up) and $P = 0.0001$ (down), two-tailed Student's *t*-test, $n = 6$–8 cells in 2 cultures. Data are mean ± s.e.m.

PD-L1 modulates sodium currents and TREK2 potassium channels via SHP-1

How does PD-L1 modulate neuronal excitability? Activation of PD-1 by PD-L1 recruits the tyrosine phosphatases SHP-1and SHP-2 (Src homology region 2 domain-containing phosphatase-1 and 2) to mediate PD-L1's biological actions in immune cells[13,39]. Immunohistochemistry shows that PD-L1 is sufficient to activate SHP-1 *in vivo* after i.t. injection, leading to increased phosphorylation of SHP-1 (pSHP-1) in mouse DRG neurons (**Fig. 6a**). In agreement, pSHP-1 colocalized with *Pd1* mRNA in DRG neurons (**Supplementary Fig. 8a**,**b**). Moreover, PD-L1-induced SHP-1 phosphorylation was blocked by the SHP-1 inhibitor sodium stibogluconate (SSG) in dissociated DRG neurons (**Supplementary Fig. 8c**). Intraplantar administration of PD-L1 induced analgesia by reducing paw withdrawal frequency in naive animals; but this analgesic effect of PD-L1 was abolished by i.pl. SSG (**Fig. 6b**). Thus, SHP-1 is not only a downstream signaling event following PD-1 activation in DRG neurons but also contributes to PD-L1-evoked analgesia.

Given an important role of sodium channels in generating action potentials and pain[40], we examined the effects of PD-L1 on transient sodium currents in mouse DRG neurons with small diameters. PD-L1 perfusion (10 ng/ml) caused a gradual and persistent inhibition of transient sodium currents (**Fig. 6c**). Moreover, PD-L1-induced inhibition of sodium currents was partially blocked by the SHP inhibitor SSG (**Fig. 6c**), supporting an involvement of SHP.

The two-pore K^+ channel TREK2 regulates RMP in DRG nociceptive neurons of rats[41]. TREK2 also expressed in mouse DRG neurons (**Supplementary Fig. 9a**). We assessed whether PD-L1 would modulate TREK2 activity in heterologous CHO cells. PD-L1 caused hyperpolarization of RMP (ΔRMP ≈ 8 mV) in CHO cells coexpressing PD-1 (encoded by *PD1*, also known as*PDCD1*) and TREK2 (encoded by *KCNK10*), but this change was blocked by SSG (**Fig. 6d**). PD-L1 also potentiated TREK2-induced currents and produced a negative shift in reversal potential in CHO cells coexpressing PD-1 and TREK2, and both these effects were abolished by SSG (**Fig. 6e**). However, PD-L1 alone was insufficient to alter the voltage-ramp currents and reversal potential in CHO cells expressing either TREK2 or PD-1 (**Supplementary Fig. 9b**). Collectively, activation of PD-1 by PD-L1 might modulate neuronal excitability by suppressing the function of sodium channels and enhancing the function of potassium channels (TREK2) via SHP-1 (**Supplementary Fig. 9c**).

Human DRG neurons express functional PD-1

A translational gap from rodents to humans has been blamed for many failures in developing pain therapeutics[42,43]. We therefore examined the PD-1 expression and function in human DRG neurons from disease-free donors, as shown in our previous studies[25,44]. PD-1 immunoreactivity was observed on the cell surface of human DRG neurons of small and large sizes, as well as in human spinal nerve axons (**Fig. 7a** and **Supplementary Fig. 10a**,**b**). This staining in human DRG and nerve sections was abolished upon blockade by the immunizing peptide (**Supplementary Fig. 10a**,**b**). Both

NF200-positive and NF200-negative axons of human spinal nerve expressed PD-1 (**Supplementary Fig. 10c**).

We found PD-1 receptor to be functional in human DRG neurons: incubation of dissociated small-diameter nociceptive neurons (30–50 µm) with PD-L1 directly altered neuronal activity. At a concentration that is effective in suppressing mouse nociceptive neuron activity (10 ng/ml; **Fig. 4a**,**b**), PD-L1 markedly inhibited the firing frequency of action potentials and further increased the threshold for action potential induction (rheobase) in human DRG neurons (**Fig. 7b**,**c**). PD-L1 also caused hyperpolarization of human nociceptive neurons by decreasing RMP (**Fig. 7d**). Additionally, PD-L1 perfusion (10 ng/ml) caused a gradual and persistent inhibition of transient sodium currents in human DRG neurons (**Fig. 7e**). Notably, PD-L1-induced inhibition of sodium currents was partially blocked by SSG in mouse DRG neurons (**Fig. 6c**) but completely blocked by SSG in human DRG neurons (**Fig. 7e**), suggesting that SHP is important in regulating PD-L1 signaling in human sensory neurons.

PD-L1 and PD-1 mask spontaneous pain and allodynia in a mouse melanoma model

Given the high expression of PD-L1 in melanoma (**Fig. 2a**), we examined the contribution of PD-L1 and PD-1 to altered pain sensitivity in a mouse model of melanoma. Intraplantar injection of mouse melanoma cells (5×10^5 cells in 20 µl) into C57BL/6 mice led to time-dependent tumor growth in a hindpaw, showing a threefold increase in paw volume 4 weeks after melanoma cell implantation (MCI-4w, **Fig. 8a**). Melanoma-bearing mice also exhibited increased PD-L1 levels in serum at MCI-4w (**Fig. 8b**). Despite profound tumor growth, we did not observe cardinal features of cancer pain, including mechanical allodynia and spontaneous pain (licking or flinching of the tumor-bearing paw) (**Fig. 8c**,**d**).

Next we tested the hypothesis that pain after melanoma could be masked by upregulated PD-L1 function. We employed several pharmacological approaches to block PD-L1–PD-1 signaling. Strikingly, local neutralization of PD-L1, by i.pl. injection of soluble PD-1 (sPD-1, 5 µg, MCI-4w) elicited marked spontaneous pain (**Fig. 8e**). The onset of spontaneous pain was very rapid: mice displayed licking and flinching behavior in melanoma-bearing paws within 10–30 min after the injection. This spontaneous pain was also phasic, showing a peak every hour for the first 3 h (**Supplementary Fig. 11a** and **Supplementary Videos 1** and **2**). The same sPD-1 treatment also induced mechanical allodynia (**Supplementary Fig. 11b**). Using a two-chamber test, we found that i.pl. sPD-1 treatment also resulted in marked conditioned place preference (CPP), an operant measurement of ongoing pain[35] (**Fig. 8f**).

Given an importance of PD-L1 in regulating the function of immune system, we also investigated the effects of sPD-1 treatment on T cell and inflammatory markers in the ipsilateral hindpaw skin surrounding melanoma and control skin in the contralateral paw. To correlate the changes in these immune markers with pain, we collected skin tissues in the acute phase, 3 h after the sPD-1 treatment, when robust allodynia and spontaneous pain had developed. MCI-4w resulted in increased levels of mRNAs encoding T cell markers (CD2, CD3), a macrophage marker (CD68) and inflammatory cytokine markers (tumor necrosis factor, interleukin-1B, interleukin-6, interferon-γ, CCL2) in the ipsilateral skin, compared with the contralateral skin (**Supplementary Fig. 12**). However, the mRNA levels of these immune and inflammatory markers did not alter after sPD-1 treatment (**Supplementary Fig. 12**). This result further indicates that sPD-1 induces pain via non-immune modulation, at least in the acute phase (first 3 h).

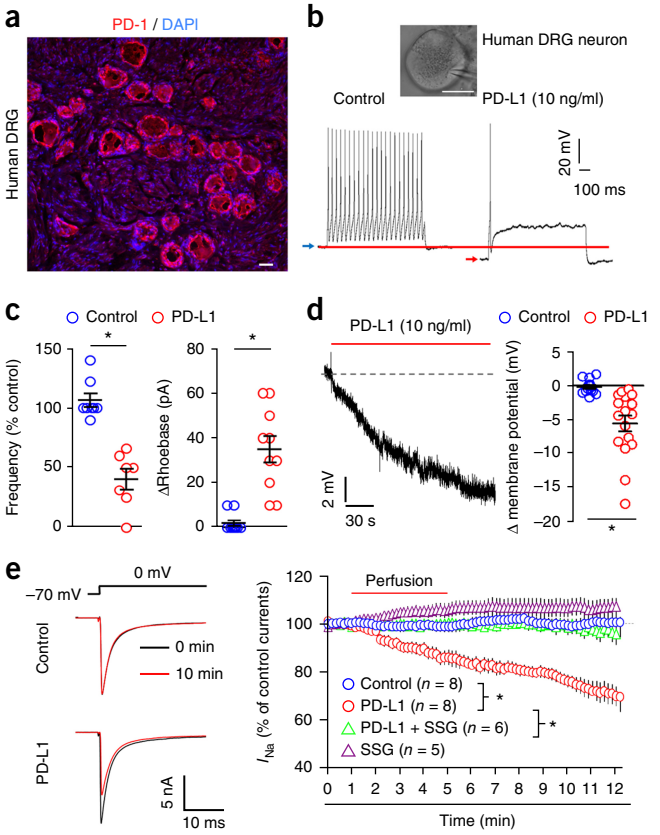

Figure 7 PD-L1 suppresses action potential firing and sodium currents and regulates RMP in human DRG neurons. (**a**) PD-1 immunostaining in a human DRG section. Blue DAPI staining labels all nuclei of cells. Scale bar, 50 µm. (**b**,**c**) *In vitro* patch-clamp recording in dissociated small-diameter human DRG neurons (30–50 µm). (**b**) Suppression of evoked action potential firing by PD-L1. Inset shows a human DRG neuron with a recording pipette. Scale bar, 25 µm. Offset between blue and red arrows shows the shift of RMP after PD-L1 treatment. (**c**) Percentage change in action potential frequency (left) and rheobase change (right) following PD-L1 perfusion (10 ng/ml). $^*P = 0.0001$ versus vehicle, two-tailed Student's *t*-test, $n = 7$–10 neurons from 3 donors. (**d**) Reduction of RMP after PD-L1 perfusion. Right, quantification of RMP change. $^*P = 0.0005$ versus vehicle, two-tailed Student's *t*-test, $n = 13$ and 17 neurons from 3 donors. (**e**) Inhibition of transient sodium currents in dissociated human DRG neurons by PD-L1 (10 ng/ml) and the effect of SSG (11 µM). Left, sodium current traces. Right, time course of relative sodium currents showing time-dependent inhibition by PD-L1. $^*P = 0.0001$, two-way repeated-measures ANOVA, $n = 5$–8 neurons from 2 donors. Data are mean ± s.e.m.

To further test the peripheral and neuronal function of PD-1 in regulating pain in melanoma, we employed a gene therapy method we recently established[27] in which small interfering RNA (siRNA) was used to knockdown PD-1 expression specifically in DRG neurons. This method allows siRNA uptake by DRG sensory neurons via axonal retrograde transport of siRNA[27]. Perisciatic injection of PD-1-targeting siRNA at MCI-4w induced marked and persistent mechanical allodynia for >4 d (**Fig. 8g**) and further evoked spontaneous pain in melanoma-bearing mice (**Fig. 8h**). Compared to nontargeting control siRNA, this *Pd1*-targeting siRNA reduced PD-1 expression in mouse DRG and sciatic nerve but not in spinal cord tissues (**Supplementary Fig. 13**). Thus, PD-1 expressed by DRG neurons could be sufficient to mask cancer pain.

Finally, we evaluated whether anti-PD-1 antibodies would also unmask pain similarly to sPD-1 and *Pd1* siRNA in the melanoma model.

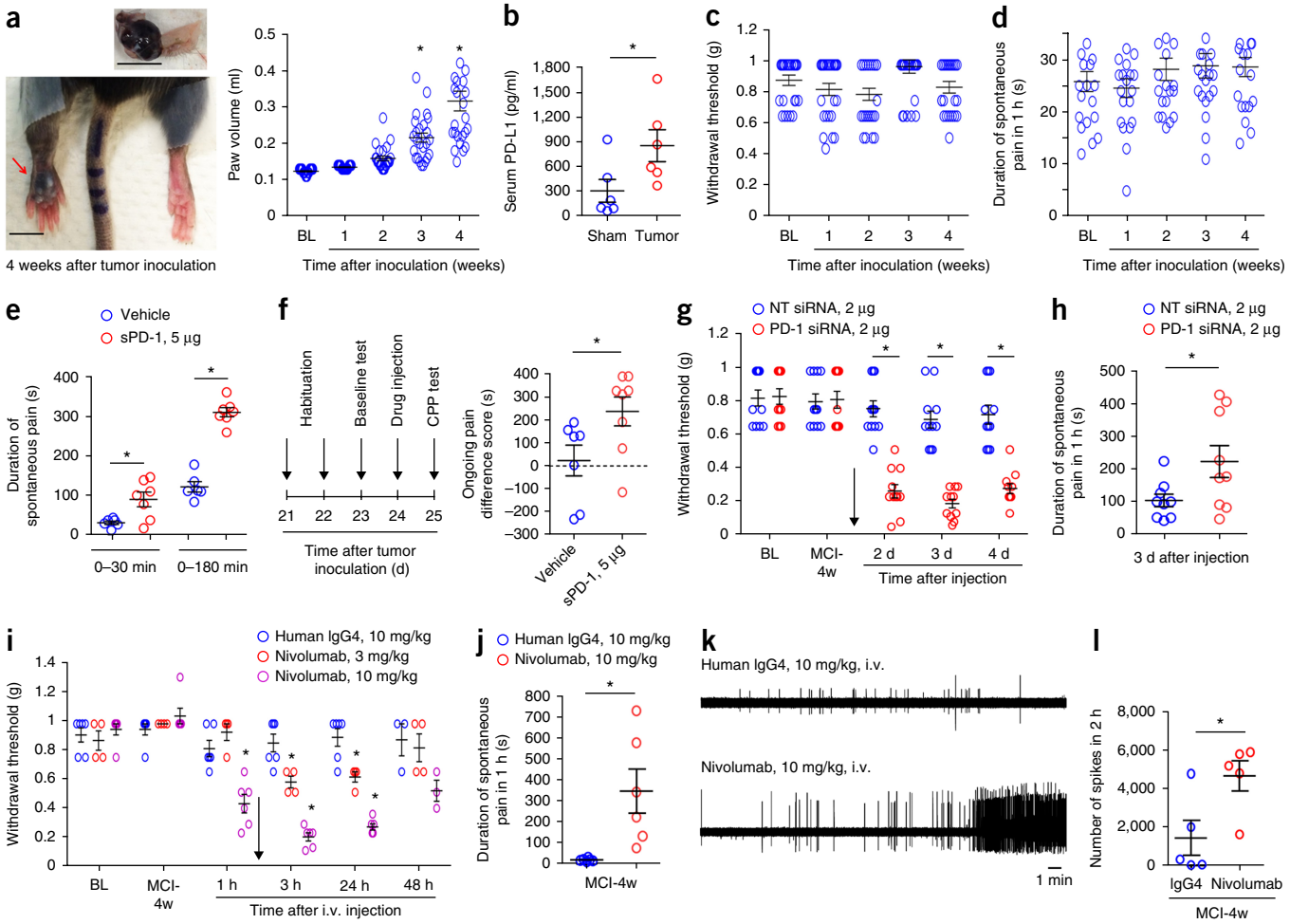

Figure 8 Blocking of PD-L1 or PD-1 signaling induces spontaneous pain and allodynia in a mouse melanoma model. (**a**) Tumor growth after melanoma cell inoculation in a hindpaw. Left, images of ipsilateral hindpaw (red arrow) and contralateral hindpaw and an isolated melanoma (top) at MCI-4w. Scale bars, 5 mm. Right, time course of tumor growth after MCI, revealed by hindpaw volume change. BL, baseline. $P = 0.0001$, one-way ANOVA, followed by Bonferroni's *post hoc* test, $^*P = 0.0001$ versus baseline (BL), $n = 25$ mice per group. (**b**) Serum PD-L1 levels in sham control mice and melanoma-bearing mice (MCI-4w). $^*P = 0.0441$, two-tailed Student's *t*-test. $n = 6$ mice per group. (**c**,**d**) Time course of mechanical pain (**c**) and spontaneous pain (duration of licking or flinching, **d**) after MCI. Note that tumor growth is not associated with the development of mechanical allodynia and spontaneous pain. $n = 21$ and 25 mice per group. (**e**) Induction of spontaneous pain by sPD-1 following i.pl. injection at MCI-4w. Note a rapid onset of spontaneous pain by sPD-1 within 30 min. $^*P = 0.0148$ (0–30 min); $P = 0.0001$ (0–180 min), compared with vehicle, two-tailed Student's *t*-test. $n = 6$ and 7 mice per group. (**f**) Induction of ongoing pain (CPP) in melanoma-bearing mice by sPD-1 (i.pl.). Left, procedure for assessing CPP in a two-chamber test. Right, difference in time spent in the drug-paired compartment between the preconditioning and postconditioning phases. $^*P = 0.0367$, two-tailed Student's *t*-test, $n = 7$ or 8 mice per group. (**g**,**h**) Induction of mechanical allodynia (**g**, $n = 11$ mice per group) and spontaneous pain (**h**, $n = 9$ mice per group) by perisciatic injection of PD-1-targeting siRNA (2 µg) but not by control nontargeting siRNA (NT, 2 µg) given at MCI-4w. $P = 0.0001$, repeated-measures two-way ANOVA, followed by Bonferroni's *post hoc* test, $^*P < 0.05$ (**g**), $^*P = 0.0373$, two-tailed Student's *t*-test (**h**). (**i**,**j**) Intravenous nivolumab (3 and 10 mg/kg), given at MCI-4w (arrow), induces mechanical allodynia (**i**, $n = 4$–6 mice per group) and spontaneous pain 3 h after injection (**j**, $n = 6$ mice per group). $P = 0.0001$, repeated-measures two-way ANOVA, followed by Bonferroni's *post hoc* test, $^*P < 0.05$ compared with control human IgG4 (**i**); $^*P = 0.0112$, two-tailed Student's *t*-test (**j**). (**k**,**l**) Intravenous nivolumab (10 mg/kg, MCI-4w) increases spontaneous firing of afferent fibers in the sciatic nerve 3 h after the injection. (**k**) Discharge traces in melanoma-bearing mice treated with nivolumab and human IgG4 control. (**l**) Number of spikes in 2 h after the treatment. $^*P = 0.0280$, two-tailed Student's *t*-test, $n = 5$ mice per group. Data are mean ± s.e.m.

Intravenous injection of nivolumab, but not the control human IgG4 (3–10 mg/kg), caused rapid, persistent and dose-dependent mechanical allodynia and also elicited marked spontaneous pain (**Fig. 8i**,**j**). Furthermore, RMP1-14, a mouse anti-PD-1 antibody (10 mg/kg intravenously (i.v.)), evoked marked spontaneous pain and mechanical allodynia (**Supplementary Fig. 14a**,**b**). *In vivo* recordings in the mouse sciatic nerve showed that i.v. nivolumab significantly increased spontaneous discharges in nerve fibers (**Fig. 8k**,**l**), indicating that anti-PD-1 treatment can unmask pain by increasing the excitability of primary afferent fibers. Moreover, local injections of nivolumab via the intrathecal or intraplantar route each evoked mechanical allodynia in melanoma-bearing mice (**Supplementary Fig. 14c**,**d**). Blocking the downstream signaling of PD-1 with the SHP-1 inhibitor SSG also elicited spontaneous pain (**Supplementary Fig. 14e**). Together, these findings suggest that PD-L1 can mask pain in nonmetastatic melanoma via PD-1 and SHP (**Supplementary Fig. 14f**).

DISCUSSION

The prevailing view is that cancers secrete pronociceptive mediators to activate or sensitize primary afferent neurons in the cancer

microenvironment. This microenvironment contains growth factors such as NGF and VEGF that cause sprouting of pain-sensing afferent fibers[3,4]. In this study, we have demonstrated that cancers also produce the anti-nociceptive mediator PD-L1 to suppress pain. In particular, we uncover PD-L1 as a previously unrecognized endogenous inhibitor of pain. PD-L1 is produce not only by melanoma but also by nonmalignant tissues such as skin, DRG and spinal cord. In naive mice, exogenous application of PD-L1 induced analgesia, whereas blockade of endogenous PD-L1 and PD-1 signaling via sPD-L1, PD-1 antibodies or *Pd1* deletion resulted in hyperalgesia. PD-L1 increased pain threshold via the PD-1 receptor, as the analgesic effect of PD-L1 was completely lost in mice lacking *Pd1*. In addition to physiological pain in naive animals, PD-L1 potently suppressed formalin-induced acute inflammatory pain. Furthermore, PD-L1 reduced chronic pain effectively, including nerve-injury-induced neuropathic pain and bone cancer pain in rodents, via both peripheral and central actions.

We have also demonstrated that PD-L1 is a neuromodulator that modulates neuronal excitability in mouse and human DRGs of the peripheral nervous system and synaptic transmission in the spinal cord of the CNS, through activation of PD-1 receptor. It is generally believed that PD-1 is expressed by immune cells such as T cells[13]. However, non-immune cells such as melanoma cells also express PD-1 (ref. 45). Our analyses using immunohistochemistry, *in situ* hybridization, and electrophysiology in dissociated DRG neurons clearly demonstrate the presence of anatomical and functional PD-1 receptor in mouse and human DRG neurons.

Mechanistically, we found that activation of PD-1 by PD-L1 inhibited action potential induction and suppressed transient sodium currents in mouse and human DRG neurons. PD-L1 also regulated RMPs and caused hyperpolarization, via PD-1 and SHP activation and subsequent activation of the two-pore K^+ channel TREK2. Furthermore, PD-L1 was present in spinal cord tissue, and bath application of PD-L1 suppressed excitatory synaptic transmission (sEPSCs) in lamina IIo neurons in the spinal cord pain circuit. PD-L1 also inhibited bone-cancer-induced hyperexcitability in spinal WDR neurons. These results strongly suggest that as a neuromodulator PD-L1 modulates pain sensitivity by both peripheral and central mechanisms. Because PD-L1 affects both the frequency and amplitude of sEPSCs in spinal cord slices (**Supplementary Fig. 6**), PD-1 may also be present in postsynaptic neurons in the spinal cord and brain. Future study is necessary to investigate signaling mechanisms by which PD-L1–PD-1 signaling regulates synaptic transmission and synaptic plasticity in the spinal cord and brain. Given the importance of immune cells in chronic pain sensitization[10,46], it is conceivable that PD-L1 could control chronic pain by suppressing T-cell activation and proinflammatory responses[47]. However, given the time scale of neuromodulation (minutes to hours), the rapid changes in pain behavior after the manipulations of the PD-L1–PD-1–SHP pathway are likely to be mediated by neuronal activation. Growing evidence supports an important role of glial cells such as microglia and astrocytes in the pathogenesis of pain[10,48–50]. We should not exclude the possibility that PD-L1 and PD-1 may also regulate glial signaling in persistent pain.

It is noteworthy that PD-L1 suppressed pathological pain not only in models of inflammatory, neuropathic and bone cancer pain but also in a melanoma model, in which mice exhibited high PD-L1 levels in circulation. We provide several lines of pharmacological and behavioral evidence to demonstrate a critical role of the PD-L1–PD-1 axis in masking pain in melanoma-bearing mice. First, inoculation of B16 melanoma cells resulted in robust melanoma growth but not in spontaneous pain or mechanical allodynia. Second, intraplantar neutralization of PD-L1 with soluble PD-1 induced spontaneous pain, ongoing pain (CPP) and mechanical allodynia, and furthermore, systemic or local injection of either human anti-PD-1 antibody (nivolumab) or mouse anti-PD-1 antibody (RMP1-14) or siRNA knockdown of PD-1 expression in DRGs each induced robust pain symptoms in the melanoma-bearing hindpaw. Finally, inhibition of SHP also evoked spontaneous pain. It will be of great interest to investigate whether PD-L1 can still mask pain after melanoma metastasis.

What is the biological significance of PD-L1 in suppressing the function of both immune system and nociceptive system? Because these two systems are important for host defense[20,21], it is conceivable that the tumor can shut off both defense systems via PD-L1 secretion for optimal host invasion and cancer growth. Emerging immune therapies with anti-PD1 and anti-PD-L1 antibodies have shown efficacy in treating cancers such as melanoma[8,15,16]. Our findings suggest the importance of examining the pain caused by individual tumor sites in patients with melanoma and other malignancies before, after and during immune therapies. Conversely, it is also of great interest to identify new types of pain inhibitors produced by cancer cells, which will open a new avenue to developing future pain medicine. Given the high potency of PD-L1 in suppressing activities of human nociceptive neurons, local targeting of PD-L1–PD-1 signaling in sensory neurons may lead to the development of new analgesics.

METHODS

Methods, including statements of data availability and any associated accession codes and references, are available in the online version of the paper.

Note: Any Supplementary Information and Source Data files are available in the online version of the paper.

ACKNOWLEDGMENTS

This study is supported by NIH RO1 grants NS87988, DE17794 and DE22743 and National Science Fund of China (NSFC) 31420103903. Y.H.K. was supported by the National Research Foundation of Korea (NRF) 2013R1A6A3A04065858.

AUTHOR CONTRIBUTIONS

G.C. developed the project, performed behavioral and histochemical experiments and prepared the final figures. Y.H.K. conducted electrophysiology in mouse and human DRG neurons. H. Li and H. Luo performed spinal cord recordings and behavioral test in bonce caner model under the guidance of Y.-Q.Z. D.-L.L. performed recordings in whole-mount mouse DRGs. Z.-J.Z. contributed to histochemistry in *Pd1* knockout mice. M.L. did some *in situ* hybridization experiment. W.C. conducted some electrophysiology in mouse DRG neurons. R.-R.J. and Y.-Q.Z. supervised the project. R.-R.J., G.C. and Y.-Q.Z. wrote the paper.

COMPETING FINANICIAL INTERESTS

The authors declare no competing financial interests.

1. Mantyh, P.W. Cancer pain and its impact on diagnosis, survival and quality of life. *Nat. Rev. Neurosci.* **7**, 797–809 (2006).
2. Mantyh, P. Bone cancer pain: causes, consequences, and therapeutic opportunities. *Pain* **154** (Suppl. 1), S54–S62 (2013).
3. Selvaraj, D. *et al.* A functional role for VEGFR1 expressed in peripheral sensory neurons in cancer pain. *Cancer Cell* **27**, 780–796 (2015).
4. Jimenez-Andrade, J.M., Ghilardi, J.R., Castañeda-Corral, G., Kuskowski, M.A. & Mantyh, P.W. Preventive or late administration of anti-NGF therapy attenuates tumor-induced nerve sprouting, neuroma formation, and cancer pain. *Pain* **152**, 2564–2574 (2011).
5. Cain, D.M. *et al.* Functional interactions between tumor and peripheral nerve: changes in excitability and morphology of primary afferent fibers in a murine model of cancer pain. *J. Neurosci.* **21**, 9367–9376 (2001).
6. Schweizerhof, M. *et al.* Hematopoietic colony-stimulating factors mediate tumor-nerve interactions and bone cancer pain. *Nat. Med.* **15**, 802–807 (2009).

7. Schmidt, B.L. The neurobiology of cancer pain. *Neuroscientist* **20**, 546–562 (2014).
8. Brahmer, J.R. *et al.* Safety and activity of anti-PD-L1 antibody in patients with advanced cancer. *N. Engl. J. Med.* **366**, 2455–2465 (2012).
9. Negin, B.P. *et al.* Symptoms and signs of primary melanoma: important indicators of Breslow depth. *Cancer* **98**, 344–348 (2003).
10. Ji, R.R., Chamessian, A. & Zhang, Y.Q. Pain regulation by non-neuronal cells and inflammation. *Science* **354**, 572–577 (2016).
11. Sharma, P. & Allison, J.P. The future of immune checkpoint therapy. *Science* **348**, 56–61 (2015).
12. Butte, M.J., Keir, M.E., Phamduy, T.B., Sharpe, A.H. & Freeman, G.J. Programmed death-1 ligand 1 interacts specifically with the B7-1 costimulatory molecule to inhibit T cell responses. *Immunity* **27**, 111–122 (2007).
13. Keir, M.E., Butte, M.J., Freeman, G.J. & Sharpe, A.H. PD-1 and its ligands in tolerance and immunity. *Annu. Rev. Immunol.* **26**, 677–704 (2008).
14. Day, C.L. *et al.* PD-1 expression on HIV-specific T cells is associated with T-cell exhaustion and disease progression. *Nature* **443**, 350–354 (2006).
15. Herbst, R.S. *et al.* Predictive correlates of response to the anti-PD-L1 antibody MPDL3280A in cancer patients. *Nature* **515**, 563–567 (2014).
16. Topalian, S.L. *et al.* Safety, activity, and immune correlates of anti-PD-1 antibody in cancer. *N. Engl. J. Med.* **366**, 2443–2454 (2012).
17. Ansell, S.M. *et al.* PD-1 blockade with nivolumab in relapsed or refractory Hodgkin's lymphoma. *N. Engl. J. Med.* **372**, 311–319 (2015).
18. Hamanishi, J. *et al.* Safety and antitumor activity of anti-PD-1 antibody, nivolumab, in patients with platinum-resistant ovarian cancer. *J. Clin. Oncol.* **33**, 4015–4022 (2015).
19. Postow, M.A. *et al.* Nivolumab and ipilimumab versus ipilimumab in untreated melanoma. *N. Engl. J. Med.* **372**, 2006–2017 (2015).
20. Talbot, S., Foster, S.L. & Woolf, C.J. Neuroimmunity: physiology and pathology. *Annu. Rev. Immunol.* **34**, 421–447 (2016).
21. McMahon, S.B., La Russa, F. & Bennett, D.L. Crosstalk between the nociceptive and immune systems in host defence and disease. *Nat. Rev. Neurosci.* **16**, 389–402 (2015).
22. Chiu, I.M. *et al.* Bacteria activate sensory neurons that modulate pain and inflammation. *Nature* **501**, 52–57 (2013).
23. Ji, R.R., Xu, Z.Z. & Gao, Y.J. Emerging targets in neuroinflammation-driven chronic pain. *Nat. Rev. Drug Discov.* **13**, 533–548 (2014).
24. Li, Y. *et al.* Toll-like receptor 4 signaling contributes to paclitaxel-induced peripheral neuropathy. *J. Pain* **15**, 712–725 (2014).
25. Xu, Z.Z. *et al.* Inhibition of mechanical allodynia in neuropathic pain by TLR5-mediated A-fiber blockade. *Nat. Med.* **21**, 1326–1331 (2015).
26. Park, C.K. *et al.* Extracellular microRNAs activate nociceptor neurons to elicit pain via TLR7 and TRPA1. *Neuron* **82**, 47–54 (2014).
27. Berta, T. *et al.* Extracellular caspase-6 drives murine inflammatory pain via microglial TNF-α secretion. *J. Clin. Invest.* **124**, 1173–1186 (2014).
28. Patel, S.P. & Kurzrock, R. PD-L1 expression as a predictive biomarker in cancer immunotherapy. *Mol. Cancer Ther.* **14**, 847–856 (2015).
29. Weber, J.S. *et al.* Nivolumab versus chemotherapy in patients with advanced melanoma who progressed after anti-CTLA-4 treatment (CheckMate 037): a randomised, controlled, open-label, phase 3 trial. *Lancet Oncol.* **16**, 375–384 (2015).
30. Brahmer, J.R., Hammers, H. & Lipson, E.J. Nivolumab: targeting PD-1 to bolster antitumor immunity. *Future Oncol.* **11**, 1307–1326 (2015).
31. Hucho, T. & Levine, J.D. Signaling pathways in sensitization: toward a nociceptor cell biology. *Neuron* **55**, 365–376 (2007).
32. Reichling, D.B. & Levine, J.D. Critical role of nociceptor plasticity in chronic pain. *Trends Neurosci.* **32**, 611–618 (2009).
33. Basbaum, A.I., Bautista, D.M., Scherrer, G. & Julius, D. Cellular and molecular mechanisms of pain. *Cell* **139**, 267–284 (2009).
34. Devor, M., Wall, P.D. & Catalan, N. Systemic lidocaine silences ectopic neuroma and DRG discharge without blocking nerve conduction. *Pain* **48**, 261–268 (1992).
35. Chen, G., Park, C.K., Xie, R.G. & Ji, R.R. Intrathecal bone marrow stromal cells inhibit neuropathic pain via TGF-β secretion. *J. Clin. Invest.* **125**, 3226–3240 (2015).
36. Todd, A.J. Neuronal circuitry for pain processing in the dorsal horn. *Nat. Rev. Neurosci.* **11**, 823–836 (2010).
37. Braz, J., Solorzano, C., Wang, X. & Basbaum, A.I. Transmitting pain and itch messages: a contemporary view of the spinal cord circuits that generate gate control. *Neuron* **82**, 522–536 (2014).
38. Yang, Y. *et al.* Delayed activation of spinal microglia contributes to the maintenance of bone cancer pain in female Wistar rats via P2X7 receptor and IL-18. *J. Neurosci.* **35**, 7950–7963 (2015).
39. Hebeisen, M. *et al.* SHP-1 phosphatase activity counteracts increased T cell receptor affinity. *J. Clin. Invest.* **123**, 1044–1056 (2013).
40. Bennett, D.L. & Woods, C.G. Painful and painless channelopathies. *Lancet Neurol.* **13**, 587–599 (2014).
41. Acosta, C. *et al.* TREK2 expressed selectively in IB4-binding C-fiber nociceptors hyperpolarizes their membrane potentials and limits spontaneous pain. *J. Neurosci.* **34**, 1494–1509 (2014).
42. Woolf, C.J. Overcoming obstacles to developing new analgesics. *Nat. Med.* **16**, 1241–1247 (2010).
43. Mogil, J.S. Animal models of pain: progress and challenges. *Nat. Rev. Neurosci.* **10**, 283–294 (2009).
44. Han, Q. *et al.* SHANK3 deficiency impairs heat hyperalgesia and TRPV1 signaling in primary sensory neurons. *Neuron* **92**, 1279–1293 (2016).
45. Kleffel, S. *et al.* Melanoma cell-intrinsic PD-1 receptor functions promote tumor growth. *Cell* **162**, 1242–1256 (2015).
46. Scholz, J. & Woolf, C.J. The neuropathic pain triad: neurons, immune cells and glia. *Nat. Neurosci.* **10**, 1361–1368 (2007).
47. Uçeyler, N. *et al.* Deficiency of the negative immune regulator B7-H1 enhances inflammation and neuropathic pain after chronic constriction injury of mouse sciatic nerve. *Exp. Neurol.* **222**, 153–160 (2010).
48. Guan, Z. *et al.* Injured sensory neuron-derived CSF1 induces microglial proliferation and DAP12-dependent pain. *Nat. Neurosci.* **19**, 94–101 (2016).
49. Grace, P.M., Hutchinson, M.R., Maier, S.F. & Watkins, L.R. Pathological pain and the neuroimmune interface. *Nat. Rev. Immunol.* **14**, 217–231 (2014).
50. Sorge, R.E. *et al.* Different immune cells mediate mechanical pain hypersensitivity in male and female mice. *Nat. Neurosci.* **18**, 1081–1083 (2015).

ONLINE METHODS

Reagents. Mouse PD-1 (catalog: 1021-PD-100) and rat IgG2A isotype control (catalog: MAB006) was obtained from R&D. Mouse PD-L1 (catalog: ab180058) and human IgG4 control (catalog: ab90286) were purchased from Abcam. Nivolumab (Opdivo), a humanized anti-PD-1 antibody, was purchased from Bristol-Myers Squibb. RMP1-14 antibody to mouse PD-1 (catalog: BE0146) was from Bio X Cell. Mouse *Pd1*-targeting siRNA (catalog: L-040330-01-0005) and nontargeting siRNA (catalog: D-0018100-01-20) were purchased from Thermo Scientific Dharmacon. RVG peptide was synthetized by Invitrogen and mixed with siRNA to increase neuronal uptake of siRNA by axons in the sciatic nerve[27]. SHP-1 inhibitor sodium stibogluconate (SSG) was from Calbiochem (catalog: 567565). The *PD1*(*PDCD1*) cDNA construct (SC117011, NM_005018) and *TREK2*(*KCNK10*) cDNA construct (SC110477, NM_021161) were purchased from Origene Technologies.

Animals. Adult mice (males, 8–10 weeks) were used for behavioral and biochemical studies. *Pd1* knockout mice with a C57BL/6 background were purchased from the Jackson Laboratory (stock no.: 021157) and maintained at the Duke animal facility. Young mice (5–7 weeks of both sexes) were used for electrophysiological studies in DRG neurons. All mouse procedures were approved by the Institutional Animal Care & Use Committee of Duke University. For the bone cancer pain experiment, adult Wistar rats (females, 8 weeks) were obtained from Shanghai Experimental Animal Center of Chinese Academy of Sciences and the rat experiments were approved by the Animal Care and Use Committee of Fudan University. All animals were housed under a 12-h light/dark cycle with food and water available *ad libitum*. No statistical method was used to predetermine sample size. No randomization was applied to the animal experiments. Sample sizes were estimated based on our previous studies for similar types of behavioral, biochemical and electrophysiological analyses[25,27,35]. Two to five mice or rats were housed in each cage. Animal experiments were conducted in accordance with the National Institutes of Health Guide for the Care and Use of Laboratory Animals. The numbers of mice and rats used in different experiments are summarized in **Supplementary Figure 15**.

Culture of murine melanoma cells. Mouse melanoma cell line B16-F10 was obtained from ATCC (ATCCCRL-6475, Rockville, Maryland). Melanoma cells were grown in Dulbecco's modified Eagle's medium containing 4,500 mg/l glucose, 100 mg/l penicillin, 100 mg/l streptomycin and 10% FBS in 5% CO_2/95% air at 37 °C. Cells were collected for experiments following enzymatic digestion with trypsin. We did not test for mycoplasma contamination after cell line purchase.

Mouse and rat models of cancer and pain. We used the following rodent models of pain.

Mouse model of melanoma. Mouse B16-F10 melanoma cells (5×10^5 cells in 20 µl, suspended in PBS) were subcutaneously injected into the plantar region of the left hindpaw of a mouse.

Mouse model of inflammatory pain. Acute inflammatory pain was induced by intraplantar injection of 20 µl diluted formalin (5%).

Mouse model of neuropathic pain. Chronic constriction injury (CCI) to induce neuropathic pain was produced under isoflurane anesthesia[35]. After the left sciatic nerve was exposed, three ligatures (7-0 Prolene) were placed around the nerve proximal to the trifurcation with 1 mm between each ligature. The ligatures were loosely tied until a short flick of the ipsilateral hind limb was observed. Animals in the sham group received surgery identical to those described but without nerve ligation.

Rat bone cancer pain model. Tumor cells were extracted from the ascitic fluid of rats that received Walker 256 rat mammary gland carcinoma cells, kindly provided by Institute of Radiation Medicine, Fudan University, and a suspension of 1×10^8/ml tumor cells in PBS was prepared. No mycoplasma testing was conducted in these cells. The inoculation was performed as previously described[38]. Briefly, rats were anesthetized with sodium pentobarbital (50 mg/kg, intraperitoneal). The right leg was shaved, and the skin was disinfected with iodine tincture and 75% ethanol. A 22-G needle was inserted at the site of the intercondylar eminence of the right tibia and was then replaced with a 10 µl microinjection syringe containing 4 µl of tumor cell suspension (4×10^5). The contents of the syringe were slowly injected into the tibial cavity. To prevent leakage of cells outside the bone, the injection site was sealed with bone wax. For the sham group (control), 4 µl of PBS was injected instead of carcinoma cells into the tibia. At the end of the experiment, radiological, postmortem and histological evaluations were performed. Rats that showed no obvious tumor growth and bone destruction after inoculation of tumor cells were excluded from the experiments.

Drug injection. For intravenous injection, anti-PD-1 antibody (nivolumab, 3 or 10 mg/kg or RMP1-14, 10 mg/kg in 100 µl PBS) or control antibody (human IgG4 or rat IgG2A) was administered into the tail vein of a mouse. For local intraplantar injection, drugs were injected in 20 µl PBS using a Hamilton microsyringe with a 30-G needle. For intrathecal injection, spinal cord puncture was made with a 30-G needle between the L5 and L6 levels to deliver reagents (10 µl) to the cerebral spinal fluid[35]. For perisciatic injection, a mixture of 2 µg siRNA and 1.5 µg of transfection reagent (chimeric rabies virus glycoprotein fragment, RVG-9R)[27] in 6 µl D5W (5% dextrose in water) was injected with a 30-G needle under the mesoneurium of the left sciatic nerve at mid-thigh level. Care was taken to avoid solution entry into the epineurium of the sciatic nerve.

***In situ* hybridization.** We used probes directed against mouse *Pdl1* (NM_021893) and *Pdcd1* (NM_008798) designed by Advanced Cell Diagnostics, and the RNAscope multiplex fluorescence assay was conducted according to the manufacturer's instructions. Prehybridization, hybridization and washing were performed according to standard methods[25].

Immunohistochemistry in mouse and human tissues and quantification. After appropriate survival times, mice were deeply anesthetized with isoflurane and perfused through the ascending aorta with PBS, followed by 4% paraformaldehyde. After the perfusion, the L4–L5 spinal cord segments, L4–L5 DRGs, sciatic nerves, and melanoma tissues were removed and postfixed in the same fixative overnight. Fresh human DRGs (L4–L5) from 4 disease-free donors from NDRI (National Disease Research Interchange)[25] and the attached spinal nerves were immediately fixed upon delivery in fresh 4% paraformaldehyde overnight. Spinal cord, DRG and nerve tissue sections 10, 14 (10 or 14 (m) and free-floating spinal cord and skin sections (30 µm) were cut in a cryostat. The sections were blocked with 2% goat or donkey serum for 1 h at room temperature and then incubated overnight at 4 °C with the following primary antibodies: anti-PD-1 (rabbit, 1:500, Sigma, catalog: PRS4065), anti-phosphorylated SHP-1 (pSHP-1, rabbit, 1:500, Abcam, catalog: ab51171), anti-NeuN (mouse, 1:1,000, Millipore, catalog: MAB377), anti-NF200 (mouse, 1:1,000, Sigma, catalog: N0142), anti-TREK2 (rabbit, 1:200, AlomoneLabs, catalog: APC-055) and anti-CGRP (goat, 1:500, Abcam, catalog: ab36001). After washing, the sections were incubated with for 2 h at room temperature with the following secondary antibodies (1:400), obtained from Jackson ImmunoResearch: Cy3-donkey anti-rabbit (catalog: 711-165-152), Cy3-donkey anti-goat (catalog: 705-165-147), FITC-donkey anti-mouse (catalog: 715-095-150), and Cy5-donkey anti-mouse (catalog: 715-175-150). For double immunofluorescence, sections were incubated with a mixture of polyclonal and monoclonal primary antibodies, followed by a mixture of Cy3- and FITC- conjugated secondary antibodies or FITC-conjugated IB4 (10 µg/ml; Sigma-Aldrich, catalog: L2895)[25]. In some cases, DAPI (1:1,000, Vector Laboratories, catalog: H-1200) or Nissl staining (1:200, ThermoFisher Scientific, catalog: N21483) was used to stain cell nuclei or neurons in tissue sections. The stained sections were examined with a Nikon fluorescence microscope, and images were captured with a CCD Spot camera. For high resolution images, sections were also examined under a Zeiss 510 inverted confocal microscope. To confirm the specificity of PD-1 antibody, blocking experiments were conducted in DRG, nerve, spinal cord and skin sections using a mixture of anti-PD-1 antibody (1:500, ~2 µg/ml) and immunizing blocking peptide (1:300, ~0.7 µg/ml; that is, ten times the molar concentration of the antibody, Sigma, catalog: SBP4065), based on a protocol recommended for blocking with immunizing peptide (http://www.abcam.com/protocols/blocking-with-immunizing-peptide-protocol-peptide-competition).

To determine whether there is neuronal loss in *Pd1* deficient mice, we conducted semi-quantification of different neuronal populations in DRGs of WT and *Pd1* knockout mice. All series L4 DRG sections (14 µm) were collected and every fifth section was used for the respective immunostaining (CGRP, NF200), IB4 staining or Nissl staining. The number of positive neurons for each staining was counted and the percentage of the labeled population was calculated based on

the Nissl-stained total population in DRG sections. To quantify immunostaining in the dorsal horn, immunofluorescence intensity in spinal cord sections of WT and knockout mice (3–5 spinal sections per mouse) were included.

ELISA. The mouse PD-L1 ELISA kit was purchased from US Biological (catalog: 027620). ELISA was performed using culture medium, serum and different normal tissues, including paw skin, sciatic nerve, gastrocnemius, DRG, brain, spinal cord, lung, thymus, kidney, spleen and liver, as well as malignant skin tissue bearing melanoma. Cultured cells and tissues were homogenized in a lysis buffer containing protease and phosphatase inhibitors. Serum was obtained from whole blood, collected by cardiac puncture. After 30 min at room temperature, the clot was removed and placed in a refrigerated centrifuge at 2,000*g* for 10 min to collect the supernatant (serum). For each ELISA assay, 50 µg proteins, 50 µl of culture medium or 50 µl of serum were used. ELISA was conducted according to manufacturer's instructions. The standard curve was included in each experiment.

Quantitative real-time RT-PCR. Hindpaw skins of MCI-4w mice were collected 3 h after the intraplantar injection. Total RNA was extracted using Direct-zol RNA MiniPrep Kit (Zymo Research Corporation) and 0.5–1 µg of RNA was reverse-transcribed using the iScript cDNA Synthesis (Bio-Rad). Specific primers including *Gapdh* control were designed using IDT SciTools Real-Time PCR software. We performed gene-specific mRNA analyses using the MiniOpticon Real-Time PCR system (Bio-Rad)[35]. Quantitative PCR amplification reactions contained the same amount of reverse transcription (RT) product, including 7.5 µL of 2× iQSYBR-green mix (Bio-Rad) and 100–300 nM forward and reverse primers in a final volume of 15 µL. The primer sequences are shown in **Supplementary Figure 12b**. Primer efficiency was obtained from the standard curve and integrated for calculation of the relative gene expression, which was based on real-time PCR threshold values of different transcripts and groups.

Western blot. Protein samples were prepared in the same way as for ELISA analysis, and 20–50 µg of proteins were loaded for each lane and separated by SDS-PAGE (4–15%; Bio-Rad). After the transfer, the blots were incubated overnight at 4 °C with polyclonal antibody against PD-1 (1:1,000, rabbit; Sigma, catalog: PRS4065). For loading control, the blots were probed with GAPDH antibody (1:20,000, mouse; Sigma, catalog: G8795). These blots were further incubated with HRP-conjugated secondary antibody and developed in ECL solution (Pierce). Specific bands were evaluated by apparent molecular sizes. The intensity of the selected bands was analyzed using NIH ImageJ software. Uncut gels for the represented blots are included in **Supplementary Figure 13**.

Whole-cell patch clamp recordings in dissociated mouse DRG neuron. DRGs were aseptically removed from mice 4–7 weeks old and digested with collagenase (0.2 mg/ml, Roche) and dispase-II (3 mg/ml, Roche) for 120 min. Cells were placed on glass cover slips coated with poly-D-lysine and grown in a Neurobasal defined medium (10% FBS and 2% B27 supplement) at 37 °C with 5% CO_2/95% air for 24 h before experiments. Whole-cell voltage clamp recordings were performed at room temperature to measure transient sodium currents and action potentials, respectively, with an EPC10 amplifier (HEKA) and an Axopatch-200B amplifier with a Digidata 1440A (Axon Instruments)[25]. The patch pipettes were pulled from borosilicate capillaries (Chase Scientific Glass Inc.). When filled with the pipette solution, the resistance of the pipettes was 4–5 MΩ. The recording chamber (300 µl) was continuously superfused (3–4 ml/min). Series resistance was compensated for (>80%) and leak subtraction was performed. Data were low-pass-filtered at 2 KHz, sampled at 10 KHz. The pClamp10 (Axon Instruments) software was used during experiments and analysis. For sodium current recording, pipette solution contained (in mM) CsCl 130, NaCl 9, $MgCl_2$ 1, EGTA 10, HEPES 10, adjusted to pH 7.4 with CsOH. The external solution was composed of (in mM) NaCl 131, TEA chloride 10, CsCl 10, $CaCl_2$ 1, $MgCl_2$ 2, $CdCl_2$ 0.3, 4-aminopyridine 3, HEPES 10, glucose 10, adjusted to pH 7.4 with NaOH. In voltage-clamp experiments, the transient sodium current (I_{Na}) was evoked by a test pulse to +0 mV from the holding potential, −70 mV (ref. 25). For action potential and resting membrane potential (RMP) recordings, pipette solution contained (in mM) potassium gluconate 126, NaCl 10, $MgCl_2$ 1, EGTA 10, Na-ATP 2 and Mg-GTP 0.1, adjusted to pH 7.3 with KOH. The external solution was composed of (in mM) NaCl 140, KCl 5, $CaCl_2$ 2, $MgCl_2$ 1, HEPES 10, glucose 10, adjusted to pH 7.4 with NaOH. In current-clamp experiments, the action potentials were evoked by current injection steps. RMP was measured without current injection.

Whole-cell patch clamp recordings in whole-mount DRGs of mice *ex vivo*. L4–L5 DRGs were carefully removed 4 d after sham surgery or CCI surgery and placed in cold oxygenated ACSF. The connective tissue was gently removed under a microscope and the ganglia were digested with a mixture of 0.4 mg/ml trypsin (Sigma) and 1.0 mg/ml type A collagenase (Sigma) for 30 min at 37 °C. The intact ganglia were then incubated in ACSF oxygenated with 95% O_2 and 5% CO_2 at 28 °C for at least 1 h before transferring them to the recording chamber. DRG neurons were visualized with a 40× water-immersion objective using a BX51WI microscope (Olympus). Whole-cell current and voltage recordings were acquired with an Axon700B amplifier. Patch pipettes (4–7 MΩ) were pulled from borosilicate glass capillaries on a P-97 puller. The recording chamber (300 µl) was continuously superfused (3–4 ml/min). Series resistance was compensated for (>80%) and leak subtraction was performed. The pipette solution contained (in mM) 140 KCl, 2 $MgCl_2$, 10 HEPES, 2 Mg-ATP, pH 7.4. Osmolarity was adjusted to 290–300 mOsm. Data were acquired with a Digidata 1322A acquisition system (Molecular Devices) using pCLAMP 9.0 software. Signals were low-pass filtered at 5 kHz, sampled at 10 kHz and analyzed offline.

Primary cultures and patch clamp recordings in human DRG neurons. Disease-free human DRGs were obtained from donors through NDRI. Postmortem L3–L5 DRGs were dissected from 5 male donors, ages 27, 31, 43, 54 and 67, and delivered in ice-cold culture medium to the laboratory at Duke University within 24–72 h of death. Upon delivery, the DRGs were rapidly dissected from nerve roots and minced in a calcium-free HBSS (Gibco). Human DRG cultures were prepared as previously reported[25]. DRGs were digested at 37 °C in humidified O_2 incubator for 120 min with collagenase type II (Worthington, 285 units/mg, 12 mg/ml final concentration) and dispase II (Roche, 1 unit/mg, 20 mg/ml) in PBS with 10 mM HEPES, pH adjusted to 7.4 with NaOH. DRGs were mechanically dissociated using fire-polished pipettes, filtered through a 100-µm nylon mesh and centrifuged (500*g* for 5 min). The pellet was resuspended and plated on 0.5 mg/ml poly-D-lysine-coated glass coverslips, and cells were grown in Neurobasal medium supplemented with 10% FBS, 2% B-27 supplement, 1% N-2 supplement and 1% penicillin/streptomycin. Whole-cell patch clamp recordings in small-diameter DRG neurons (<50 µm) were conducted at room temperature using patch pipettes with resistances of 2–3 M. The recording chamber was continuously superfused (3–4 ml/min). The data were acquired at a rate of 10 kHz and filtered at 3 kHz using an EPC-10 amplifier (HEKA, Germany) and an Axopatch-200B amplifier with a Digidata 1440A (Axon Instruments). For sodium-current recording, pipette solution contained (in mM) CsCl 130, NaCl 9, $MgCl_2$ 1, EGTA 10, HEPES 10, adjusted to pH 7.4 with CsOH. The external solution was composed of (in mM) NaCl 131, TEA chloride 10, CsCl 10, $CaCl_2$ 1, $MgCl_2$ 2, $CdCl_2$ 0.3, 4-aminopyridine 3, HEPES 10, glucose 10, adjusted to pH 7.4 with NaOH. In voltage-clamp experiments, the transient sodium current (I_{Na}) was evoked by a test pulse to 0 mV from the holding potential of −70 mV. Pretreatment of the SHP-1 inhibitor SSG was performed 30 min before whole-cell patch-clamp recordings. For action potential and RMP recordings, pipette solution contained (in mM) potassium gluconate 126, NaCl 10, $MgCl_2$ 1, EGTA 10, Na-ATP 2 and Mg-GTP 0.1, adjusted to pH 7.3 with KOH. The external solution was composed of (in mM) NaCl 140, KCl 5, $CaCl_2$ 2, $MgCl_2$ 1, HEPES 10, glucose 10, adjusted to pH 7.4 with NaOH. In current-clamp experiments, the action potentials were evoked by a current injection[25]. The resting membrane potential was measured without a current injection.

CHO cell culture, transfection and electrophysiology. The CHO cell line was purchased from the Duke Cell Culture Facility. After cell line purchase, no mycoplasma testing was performed. Cells were cultured in high-glucose (4.5 g/L) Dulbecco's modified Eagle's medium containing 10% (vol/vol) FBS (Gibco). Transfection (1 µg cDNA) was performed with Lipofectamine 2000 reagent (Invitrogen) at 70% confluency and the transfected cells were cultured in the same growth medium for 48 h before electrophysiological and biochemical studies. *PD1* (*PDCD1*) cDNA construct (SC117011, NM_005018)

doi:10.1038/nn.4571

and *TREK2* (*KCNK10*) cDNA construct (SC110477, NM_021161) were purchased from Origene Technologies.

Whole-cell patch clamp recordings in transfected CHO cells were conducted at room temperature using patch pipettes with resistances of 5–6 M. The recording chamber was continuously superfused (3–4 ml/min). The data were acquired at a rate of 10 kHz and filtered at 3 kHz using an EPC-10 amplifier (HEKA, Germany). Pipette solution contained (in mM) potassium gluconate 126, NaCl 10, $MgCl_2$ 1, EGTA 10, Na-ATP 2 and Mg-GTP 0.1, adjusted to pH 7.3 with KOH. The external solution was composed of (in mM) NaCl 140, KCl 5, $CaCl_2$ 2, $MgCl_2$ 1, HEPES 10 and glucose 10, adjusted to pH 7.4 with NaOH. In voltage-clamp recordings, TREK2-induced currents were elicited by voltage ramp from −120 mV to +100 mV every 10s. In current-clamp experiments, the resting membrane potential was measured without any membrane potential compensation.

Spinal cord slice preparation and patch clamp recordings in mice *ex vivo*. The L3–L5 lumbar spinal cord segment was removed from mice under urethane anesthesia (1.5–2.0 g/kg, i.p.) and kept in preoxygenated ice-cold ACSF solution composed of (in mM) NaCl 126, KCl 3, $MgCl_2$ 1.3, $CaCl_2$ 2.5, $NaHCO_3$ 26, NaH_2PO_4 1.25 and glucose 11. Transverse slices (300–400 μm) were cut on a vibrating microslicer. The slices were perfused with ACSF solution for at least 1 h before experiment. The whole cell patch-clamp recordings were made from lamina IIo neurons in voltage clamp mode[27]. After establishing the whole-cell configuration, neurons were held at −60 mV to record spontaneous EPSCs (sEPSCs) in the presence of 10 μM picrotoxin and 2 μM strychnine. Miniature EPSCs were recorded in some neurons in the presence of 10 μM picrotoxin, 2 μM strychnine and 0.5 μM tetrodotoxin. The resistance of a typical patch pipette was 5–6 M. Signals were filtered at 2 kHz and digitized at 10 kHz. The recording data were analyzed using Mini Analysis (Synaptosoft Inc.).

Spontaneous discharge recordings in mouse sciatic nerve *in vivo*. Adult male mice (25–32g) were anesthetized with urethane (1.5 g/kg, i.p.) and monitored for loss of hind paw pinch reflex with additional injections of urethane (0.2 g/kg). The animals were artificially ventilated with oxygen on a respirator. The left thigh was shaved and an incision made parallel to the femur. The muscle was parted by blunt forceps dissection to expose the sciatic nerve proximal to the trifurcation. A cuff electrode (Microprobes) was placed loosely around the full circumference of the sciatic nerve. Skin flaps were raised to enclose a pool of mineral oil that covered the exposed regions of nerve. Spontaneous discharges in the sciatic nerve were recorded with a microelectrode AC amplifier (1800, A-M Systems), filtered (low cut-off 100 Hz and high cut-off 20 kHz), and digitized at 20 kHz (Digidata 1440A, Molecular Devices). Data were stored on a personal computer using pCLAMP 10 software and analyzed with Offline Sorter software (Plexon, Dallas, TX) and Origin pro 8.0 (Origin Lab). Sciatic nerve spikes were characterized as previously reported[25].

Extracellular recording in rat spinal cord *in vivo*. Rats were anesthetized with urethane (1.5 g/kg, i.p.), and the trachea was cannulated to allow artificial respiration. A laminectomy was performed at vertebrae T13–L1 to expose the lumbar enlargement of the spinal cord. An intrathecal catheter (PE-10) was made for drug injection. The vertebral column was rigidly fixed in the frame with clamps. The exposed spinal cord was covered with warm (37 °C) saline solution. After surgery, the animal was immobilized and artificially ventilated (Capstar-100, IITC Life Science, USA). End-tidal CO_2 was maintained at 3.5–4.5% and rectal temperature at 37–38 °C by a feedback-controlled heating blanket. The electrocardiogram was monitored and the heart rate maintained at 250–300 beats/min. Single-unit extracellular recordings were made as we reported previously[38] at L4–L5 segments 300–700 μm from the surface of the spinal cord with a glass micropipette filled with 0.5 M sodium acetate (impedance 8–10 MΩ at 1,000 Hz). The micropipette was inserted perpendicularly to the spine into the dorsal horn from a point about midway between the midline and medial edge of the dorsal root entry zone. Each neuron was functionally identified as a wide dynamic range (WDR) neuron on the basis of its responses to innocuous or noxious mechanical stimulation to the receptive fields in the plantar region of the hindpaw. WDR neurons responding to innocuous stimulation and, to a greater degree, noxious stimulation of the receptive field were analyzed in the present study. The recorded signals were amplified with a microelectrode amplifier (1800 A-M Systems, USA) and fed to a computer via a CED 1401 interface for offline analysis using Spike 2 software (Cambridge Electronic Design, Cambridge, UK). For low-intensity mechanical stimulation, graded stimuli with von Frey filaments (4, 8, 15 and 26 g) were applied for 15s at 30-s intervals. High-intensity stimulation with pinch produced by a clip (150g) was also applied for 15 s. In pharmacological studies, only one cell was studied in each animal.

Measurement of hindpaw melanoma growth in mice. To assess tumor growth after melanoma cell implantation, paw volume was determined by a water-displacement plethysmometer (Ugo Basile, Italy). The plethysmometer is a microcontrolled volume meter designed for accurate measurement of rodent paw swelling. It consists of a water-filled Perspex cell into which the paw is dipped. A transducer of original design records small differences in water level caused by volume displacement. The digital read-out shows the exact volume of the paw.

Behavioral analysis in mice and rats. The following behavioral measurements were conducted in a blinded manner and during daytime (light cycle), normally starting at 9 a.m.

Spontaneous pain in mouse melanoma model. We measured the time (in seconds) mice spent licking or flinching the melanoma-bearing hindpaws for 1 or 3 h.

Von Frey test for mechanical pain. Animals were habituated to the testing environment daily for at least 2 d before baseline testing. The room temperature and humidity remained stable for all experiments. For testing mechanical sensitivity, we confined mice in boxes placed on an elevated metal mesh floor and stimulated their hindpaws with a series of von Frey hairs with logarithmically increasing stiffness (0.02–2.56g, Stoelting), presented perpendicularly to the central plantar surface. We determined the 50% paw withdrawal threshold by the up-down method[35].

Hargreaves test for thermal pain. Thermal sensitivity was tested using Hargreaves radiant heat apparatus (IITC Life Science). The basal paw withdrawal latency was adjusted to 9–12 s, with a cutoff of 20 s to prevent tissue damage[35].

Hot plate test for thermal pain. Mice were placed on the hot plate at 50, 53 or 56 °C and the reaction time was scored when the animal began to exhibit signs of pain avoidance such as jumping or paw licking. Animals that did not respond to the noxious heat stimulus after 40 s were removed from the plate.

Analgesiometer test for mechanical sensitivity. A Randall-Selitto analgesiometer (Ugo Basile, Italy) was used to examine mechanical sensitivity by applying ascending pressure to a mouse tail, with a cutoff threshold of 250 g to avoid tissue damage.

Conditioned place preference (CPP) test for spontaneous (ongoing) pain. We used a single-trial conditioning protocol to measure CPP[35]. All mice underwent 3d of preconditioning habituation and animal behavior was video-recorded. Analyses of the preconditioning (baseline) behavior showed no pre-existing chamber preference. On the conditioning day, mice received the vehicle (PBS, 20 μl, i.pl.) paired with a randomly chosen chamber in the morning, and PD-1 (5 μg in 20 μl PBS, i.pl.) paired with the other chamber 4 h later. Chamber pairings were counterbalanced. On the test day, 20 h after the afternoon pairing, mice were placed in the CPP test box with access to both chambers and the behavior was recorded for 15 min and analyzed by ANY-maze software for chamber preference.

Statistical analyses. All data were expressed as mean ± s.e.m., as indicated in the figure legends. The sample size for each experiment was based on our previous studies on such experiments[25,35]. Statistical analyses were completed with Prism GraphPad 6.0. Biochemical and behavioral data were analyzed using two-tailed Student's *t*-test (two groups) or two-way ANOVA followed by *post hoc* Bonferroni test. Electrophysiological data were tested using one-way ANOVA (for multiple comparisons) or two-way ANOVA (for multiple time points) followed by *post hoc* Bonferroni test or Student's *t*-test (two groups). The criterion for statistical significance was $P < 0.05$. A **Supplementary Methods Checklist** is available.

Data availability. The data that support the findings of this study are available from the corresponding author upon reasonable request.